New Modified and Extended Stability Functions for the Stable Boundary Layer based on SHEBA and Parametrizations of Bulk Transfer Coefficients for Climate Models

Vladimir M. Gryanik

*Alfred-Wegener-Institut Helmholtz-Zentrum für Polar- und Meeresforschung, Bremerhaven, Germany,
and A. M. Obukhov Institute of Atmospheric Physics, Russian Academy of Sciences, Moscow, Russia*

Christof Lüpkes

Alfred-Wegener-Institut Helmholtz-Zentrum für Polar- und Meeresforschung, Bremerhaven, Germany

Andrey Grachev

*NOAA/Physical Sciences Laboratory, and Cooperative Institute for Research in Environmental Sciences,
University of Colorado Boulder, Boulder, Colorado*

Dmitry Sidorenko

Alfred-Wegener-Institut Helmholtz-Zentrum für Polar- und Meeresforschung, Bremerhaven, Germany

(Manuscript received 18 September 2019, in final form 15 May 2020)

ABSTRACT

Climate models still have deficits in reproducing the surface energy and momentum budgets in Arctic regions. One of the reasons is that currently used transfer coefficients occurring in parameterizations of the turbulent fluxes are based on stability functions derived from measurements over land and not over sea ice. An improved parameterization is developed using the Monin–Obukhov similarity theory (MOST) and corresponding stability functions that reproduce measurements over sea ice obtained during the Surface Heat Budget of the Arctic Ocean (SHEBA) campaign. The new stability functions for the stable surface layer represent a modification of earlier ones also based on SHEBA measurements. It is shown that the new functions are superior to the former ones with respect to the representation of the measured relationship between the MOST stability parameter and the bulk Richardson number. Nevertheless, the functions fulfill the same criteria of applicability as the earlier functions and contain, as an extension, a dependence on the neutral-limit turbulent Prandtl number. Applying the new functions we develop an efficient noniterative parameterization of the near-surface turbulent fluxes of momentum and heat with transfer coefficients as a function of the bulk Richardson number (Ri_b) and roughness parameters. A hierarchy of transfer coefficients is recommended for weather and climate models. They agree better with SHEBA data for strong stability ($Ri_b > 0.1$) than previous parameterizations and they agree well with those based on the Businger–Dyer functions in the range $Ri_b \leq 0.1$.

1. Introduction

The atmospheric boundary layer is often stably stratified. This holds especially for polar regions but also for other regions on Earth where stable stratification is a very common feature, e.g., during night.

However, turbulent processes in the stable boundary layer (SBL) are still poorly represented in climate and weather prediction models. In this work we study such processes with a focus on the parameterization of the turbulent surface-layer fluxes in the SBL. One of the key questions is if an improvement of the parameterization of bulk transfer coefficients for momentum, heat and other scalars is possible. Any progress would help to gain a more realistic treatment of the SBL in models.

ⓐ Denotes content that is immediately available upon publication as open access.

Corresponding author: Vladimir M. Gryanik, vladimir.gryanik@awi.de

Publisher's Note: This article was revised on 11 February 2021 to designate it as open access.

In the past, large efforts were invested in measurements of the SBL fluxes. For Arctic ocean conditions, fluxes became available, e.g., from data of the Surface Heat Budget of the Arctic Ocean (SHEBA) campaign (Uttal et al. 2002) representing measurements over about 1 year. They were obtained from sonic anemometers installed at a 20 m tower in five levels (Andreas et al. 1999; Uttal et al. 2002; Grachev et al. 2007a, hereafter G2007a). Due to the high quality of the data and since they were collected over polar oceans with frequent stable conditions, they represent an excellent dataset for developing stability functions for the SBL in the framework of the Monin–Obukhov similarity theory (MOST). Such functions were derived by G2007a.

During the pre-SHEBA epoch Andreas (2002) recommended the stability functions of Holtslag and De Bruin (1988) for use in very stable conditions in polar regions. However, the latter stability functions do not allow persistence of turbulence at a bulk Richardson number $Ri_b \geq 0.43$ [see definition of Ri_b in Eq. (22)]. This is in contradiction to results of the more recent field measurements during SHEBA and to many earlier empirical data. Based on the SHEBA data Grachev et al. (2013) showed that turbulent flow can prevail also when the critical Richardson number, defined as a threshold for the change from a Kolmogorov to a non-Kolmogorov regime, is exceeded by far (see also section 4). They observed turbulence for large values of up to 100 of the stability parameter $\zeta = z/L$, where L is the Obukhov length [see definition in Eq. (1) in section 2]. This corresponds to a bulk Richardson number Ri_b up to 0.7–1.0.

Each of the available stability functions has its own region of applicability (confidence range, see section 4). However, the advantage of the G2007a functions is that they are valid for the widest stability range $0 \leq \zeta < 100$ for which data are nowadays available. It covers the near-neutral limit of $0 \leq \zeta < 0.02$, the weakly stable range $0.02 \leq \zeta < 0.6$, the very stable range $0.6 \leq \zeta < 50$, and the extremely stable range $\zeta \geq 50$ (G2007a; Sorbjan and Grachev 2010). For the very stable and extremely stable ranges only the functions of G2007a are available. Recently, Srivastava et al. (2020) showed that the functional form of the G2007a approach is well applicable also over land and results agree after adjustment of constants better with observations obtained over an Indian land site than previous functions. Thus, the SHEBA results might have a more general meaning than expected.

However, studies applying the above-mentioned SHEBA based field observations and theoretical findings to weather prediction and climate models are still missing. One can ask the question, Why have not the stability functions of G2007a with their obvious advantages been implemented (with exception of Andreas et al.

2010a,b) in such models or in further parameterizations in the decade since their discovery? The answer consists probably in the general recognition that the application of the G2007a functions results in weaker turbulence in the range $0.1 < Ri_b < 0.2$ compared with the application of other functions. Thus, their use in models introduces an undesirable decrease of turbulent mixing, so that it does not help to solve the well known problems of nocturnal boundary layer decoupling over land (Louis 1979) and of a too weak life cycle of atmospheric cyclones in polar regions (Jung et al. 2016; Vihma et al. 2014). On the contrary, the use of the G2007a functions would make the solution of these problems even more difficult. Indeed, the functions of G2007a provide almost the lowest surface fluxes in the above mentioned stability range from all currently known empirical nonlinear stability functions, including the functions of Holtslag and De Bruin (1988), Beljaars and Holtslag (1991), and of Chenge and Brutsaert (2005). To the best of our knowledge, smaller fluxes are provided only by the empirical functions of Businger–Dyer (Businger et al. 1971; Dyer 1974), and by theoretically derived stability functions of Sukoriansky (2008), which are based on the quasi-normal scale elimination (QNSE) theory of stratified turbulence (Sukoriansky 2008, and references therein).

Thus, the straightforward implementation of the G2007a functions will definitely cause difficulties since other parameters need to be tuned to compensate for the reduction of surface-layer mixing. However, the implementation can be desirable from another point of view. For example, reduced turbulent mixing in the SBL can help to avoid an often occurring overestimation of the boundary layer height. This problem was documented in simulations by Delage (1997) and later by Sandu et al. (2013).

Assuming that the functions of G2007a are universally applicable and that they correctly represent the main physics of turbulent mixing in stably stratified flows, one can use them in models independent on the location for all regions of Earth when the prerequisites of MOST are fulfilled. Consequent model biases in the momentum and heat budgets should be related to other physical mechanisms of ice–atmosphere interaction than the turbulent mixing represented by the stability functions. Such mechanisms are, e.g., form drag, gravity wave generation, and radiative-cooling-generated mixing. These factors can have probably large impact on turbulent fluxes, but we do not consider them in this work. One can draw the clear conclusion that the implementation and at least testing of the G2007a stability functions in climate and weather predictions models is very desirable.

There are several strategies for the implementation of new parameterizations. One strategy has been repeatedly announced by several authors, e.g., Jung et al. (2016),

Vihma et al. (2014), and Mauritsen (2011). It states that a single representative pair of stability functions is universally applicable for stable stratification ($\zeta > 0$) only dependent on land or ocean but without any other dependence on location. A complementary strategy would be to account additionally for the stability over polar sea ice (Jiménez et al. 2012). However, to the best of our knowledge, even such a compromise version applying the G2007a functions over sea ice has not yet been realized. As a third strategy (see Gryanik and Lüpkes 2018) it is worth testing the stability functions of G2007a everywhere thus also in other regions than over polar sea ice. This strategy is supported by the recent work of Srivastava et al. (2020) (see above) showing the applicability of the G2007a functions also over land.

For the implementation of the stability functions in contemporary weather prediction and climate models the derivation of normalized transfer coefficients f_m and f_h and transfer coefficients C_d and C_h is required because these coefficients are the main ingredients of surface-layer schemes in the models. For practical applications noniterative parameterizations of the transfer coefficients are preferable. Often, the derivation of noniterative parameterizations of the transfer coefficients is based on MOST. This approach goes back to a method proposed by Deardorff (1968) adjusted later by Paulson (1969) and Louis (1979) for practical use in weather prediction and climate models. Recently, Gryanik and Lüpkes (2018) have further developed this method and applied it to the stability functions of G2007a.

The approach requires solving the governing MOST equation [defined later in Eq. (21)] for the stability parameter ζ in terms of the bulk Richardson number Ri_b and roughness parameters $\varepsilon_m = z/z_0$ for momentum and $\varepsilon_t = z/z_t$ for heat. However, as we will show, the G2007a functions do not approximate the observed stability parameter–bulk Richardson number relationship well especially for $\mathrm{Ri}_b < 0.1$ and lead to an overestimation of drag coefficients in the range $\mathrm{Ri}_b > 0.2$. This finding motivated us to search for new stability functions, which are able to represent both the observed flux–nondimensional gradient relationship and the ζ–Ri_b relationship simultaneously and additionally allow the approximation of stability dependent transfer coefficients for heat and momentum with better agreement to measurements.

Moreover, it is difficult to implement the stability functions of G2007a in weather prediction and climate models due to another, more technical reason. Namely, the functions are rather cumbersome. For example, they are inconvenient for numerical iterative algorithms [five iterations are typically necessary for the algorithm of

Andreas et al. (2010b)]. And their use is inconvenient to establish semianalytical methods for the parameterization of bulk transfer coefficients (Gryanik and Lüpkes 2018). Also the analytical formulation, e.g., of applicability criteria for the stability functions, is complicated when these functions are used (Sharan and Kumar 2010). The complex functional form of the stability functions complicates the qualitative interpretation of results based on physical characteristics of turbulence, such as mixing lengths and eddy diffusivities.

For these reasons a further goal of this study is to suggest new stability functions, which have a simpler functional form than the G2007a functions. Furthermore, we adjust the method proposed by Gryanik and Lüpkes (2018) for a noniterative scheme to these new functions.

To summarize, the main goals of our research are a modification and extension of the stability functions of G2007a, and finally the derivation of new noniterative parameterizations of the bulk transfer coefficients for momentum and heat on the basis of the new modified and extended stability functions.

Finally, we stress that the new stability functions that will be proposed are conceptually similar to G2007a because they are based on the same data (SHEBA). However, they represent a reformulation of findings of G2007a and, furthermore a fit to the SHEBA data of similar quality as the G2007a functions. For this reason they should be understood as an alternative to the original G2007a functions. They allow also reducing the complexity of flux parameterizations and help thus reducing excessive numerical costs when they are applied to climate models. We also stress that the newly derived noniterative parameterizations are well suited for practical applications. Their implementation is easier, especially in models already using noniterative parameterizations, such as the models of the European Centre for Medium-Range Weather Forecasts (ECMWF), the Consortium for Small-Scale Modeling (COSMO; Doms et al. 2011) used by the German Weather Service (DWD) and model ECHAM6 (Giorgetta et al. 2012), the atmosphere component of MPI-ESM (Stevens et al. 2013), and ECHAM6–Finite Element Sea Ice Ocean Model (FESOM) (Sidorenko et al. 2015) climate models, just to mention a few.

2. Background of MOST

Currently, the momentum and heat fluxes in the stable surface layer are described by the MOST (Monin and Obukhov 1954; Monin and Yaglom 1971; Foken 2006) or by the specifically generalized MOST for stable conditions (the generalized MOST in the following), see, e.g., the theories of Nieuwstadt (1984), Sorbjan (1987, 2017),

Zilitinkevich et al. (2013), and Sukoriansky and Galperin (2013). Our focus is on the classical MOST. Its validity is limited to the turbulent fluxes in the lowest part of the atmospheric boundary layer where they are assumed to be independent on height z above an underlying horizontally homogeneous surface at $z = 0$. A further assumption is that turbulence is statistically stationary. Under these limitations, in the framework of MOST all the statistics of a turbulent flow are universal functions of the single stability parameter $\zeta = z/L$, where L is the Obukhov length scale. It combines the fluxes of momentum τ and heat H. Parameters ζ and L are given as

$$\zeta = \frac{z}{L}, \quad L = \frac{u_*^2}{\kappa(g/\Theta)\theta_*} = -\frac{(\tau/\rho)^{3/2}}{\kappa(g/\Theta)(H/\rho c_p)}. \quad (1)$$

In Eqs. (1) the friction velocity u_* and temperature scale θ_* are related with the absolute value $\tau = |\boldsymbol{\tau}| = (\tau_x^2 + \tau_y^2)^{1/2}$ of momentum flux $\boldsymbol{\tau}$ as

$$\tau = \rho u_*^2, \quad (2)$$

and with heat flux H such that

$$H = -\rho c_p u_* \theta_*, \quad (3)$$

where c_p is the specific heat at constant pressure, ρ is air density, κ is the von Kármán constant (set equal to 0.4), g is the acceleration due to gravity, and Θ is either the virtual potential temperature at some reference level or the average surface-layer temperature.

In general, MOST is formulated for all moments of the flow field (Monin and Yaglom 1971). The first-order moments are the mean wind speed $U(z)$ and mean potential temperature $\Theta(z)$. For their gradients MOST states that

$$\frac{\kappa z}{u_*}\frac{\partial U}{\partial z} = \phi_m(\zeta) \quad (4)$$

and

$$\frac{\kappa z}{\theta_*}\frac{\partial \Theta}{\partial z} = \phi_h(\zeta), \quad (5)$$

where $\phi_m(\zeta)$ and $\phi_h(\zeta)$ are the MOST nondimensional universal stability functions for momentum and heat, respectively. It is assumed that the flux–gradient relationships (4) and (5) (often called flux–profile relationship) represent the data with a reasonably good accuracy for the relevant ranges of the stability parameter ζ. The functions (4) and (5) are the main ingredients of MOST, and are normalized as

$$\phi_m(0) = 1 \quad (6)$$

and

$$\phi_h(0) = \mathrm{Pr}_0 \quad (7)$$

in our study (please see appendix B for details). The parameter $\mathrm{Pr}_0 = \mathrm{Pr}(0)$ is the neutral-limit turbulent Prandtl number Pr, which is defined as

$$\mathrm{Pr} = \frac{\overline{w'u'}(\partial\Theta/\partial z)}{\overline{w'\theta'}(\partial U/\partial z)} = \frac{\phi_h(\zeta)}{\phi_m(\zeta)}. \quad (8)$$

This number characterizes the ratio of the momentum diffusion coefficient $K_m = -\overline{w'u'}/(\partial U/\partial z)$ to the scalar diffusion coefficient $K_h = -\overline{w'\theta'}/(\partial\theta/\partial z)$. If mixing of momentum and scalars have the same efficiency, i.e., $K_m = K_h$, one has $\mathrm{Pr} = 1$. It is the case of the Reynolds analogy for turbulent mixing. If $\mathrm{Pr} < 1$, the turbulent scalar diffusion is more efficient than momentum diffusion and vice versa for $\mathrm{Pr} > 1$.

Using MOST, the profiles of wind speed $U(z)$ and potential temperature $\Theta_v(z)$ can be determined. They are derived by integrating Eqs. (4) and (5). The resulting flux–profile relationships read as

$$U(z) = \frac{u_*}{\kappa}[\ln\varepsilon_m - \psi_m(\zeta) + \psi_m(\zeta/\varepsilon_m)], \quad (9)$$

$$\Theta(z) - \Theta_0 = \frac{\theta_*}{\kappa}[\mathrm{Pr}_0\ln\varepsilon_t - \psi_h(\zeta) + \psi_h(\zeta/\varepsilon_t)], \quad (10)$$

with separate neutral and nonneutral contributions. The first are represented by logarithmic terms depending on the roughness parameters $\varepsilon_m = z/z_0$ and $\varepsilon_t = z/z_t$, where z_0 and z_t are the aerodynamic roughness lengths for momentum and heat. The nonneutral contributions consist of stability correction functions for momentum $\psi_m(\zeta)$ and heat $\psi_h(\zeta)$ (often also called integrated stability functions). They are related to the stability functions by the following equations (cf. Paulson 1970):

$$\psi_k(\zeta) = \int_0^\zeta \frac{I_k - \phi_k(\zeta')}{\zeta'} d\zeta', \quad \phi_k(\zeta) = I_k - \zeta\frac{d\psi_k}{d\zeta},$$
$$k = [m, h], \quad (11)$$

with $I_m = 1$ for momentum and $I_h = \mathrm{Pr}_0$ for heat. In stable conditions $\psi_k < 0$, and vice versa $\psi_k > 0$ for unstable conditions. In the neutral case

$$\psi_k(0) = 0, \quad (12)$$

so that no correction exists by definition. The magnitude of the aerodynamic roughness lengths z_0 and

z_t is related to the height and width of the roughness elements and to hot/cold spots on the underlying surface. There are relationships in the literature for the determination of the z_0/z_t ratio over sea ice (e.g., Andreas 1987; Andreas et al. 2010a,b). However, there is not yet an overall accepted formulation. If so, very often z_0 and z_t are considered in polar research as constant values. We adopt this assumption in our research as well.

MOST becomes a closed theory when the stability functions are given. However, MOST itself does not provide these functions. Universal stability functions must be determined from precise laboratory experiments, accurate field measurements, appropriate numerical simulations, and convincing theoretical arguments. In the case of well developed turbulence the well known Businger–Dyer stability functions (Businger et al. 1971; Dyer 1974) approximate the measured data well at near-neutral and weak stability, i.e., for small values of $\zeta \leq O(1)$. The Businger–Dyer functions depend linearly on ζ with

$$\phi_m(\zeta) = 1 + a_m\zeta, \quad \phi_h(\zeta) = \mathrm{Pr}_0(1 + a_h\zeta), \quad 0 \leq \zeta < 1, \tag{13}$$

where a_m and a_h are empirical constants approximating most of the known experimental data, if representative values $a_m = a_h = 5.0$ and $\mathrm{Pr}_0 = 1$ are used. However, in literature the documented range of a_m and a_h is from 4 to 8 (Högström 1988, 1996) and Pr_0 is not always equal to 1.

Corresponding to (13) the stability correction functions $\psi_m(\zeta)$ and $\psi_h(\zeta)$ are also linear functions of ζ with

$$\psi_m(\zeta) = -a_m\zeta, \quad \psi_h(\zeta) = -\mathrm{Pr}_0 a_h\zeta, \quad 0 \leq \zeta < 1. \tag{14}$$

In general, the stability functions $\phi_k(\zeta)$ and stability correction functions $\psi_k(\zeta)$ are, however, nonlinear functions in ζ. But it is important to stress that both functions (13) and (14) describe any given stability function in the limit of small $\zeta \to 0$. Practically, this limit holds for $0 < \zeta < 0.08$ (see, e.g., Grachev et al. 2015).

At present, there is no consensus in literature about the correct functional form of stability functions beyond $\zeta \approx 3$–5 (Ri ≈ 0.2–0.25 and Ri$_f \approx 0.2$–0.25; see Grachev et al. 2013), i.e., in the region of very strong and extremely strong stability. In this range different researchers suggest nonlinear stability functions, which differ essentially from each other (Holtslag and De Bruin 1988; Beljaars and Holtslag 1991; Chenge and Brutsaert 2005; G2007a). These functions given in appendix A as well as all other ones mentioned in this study are shown in Figs. 1 and 2 .

The figures demonstrate moreover that the scatter is large not only between the empirical stability functions, but also the theoretically derived and empirical functions differ strongly from each other. As an example, we show in the same Figs. 1a and 2a the stability functions of Sukoriansky (2008) (see appendix A) derived on the basis of spectral QNSE theory for stably stratified turbulence (Sukoriansky and Galperin 2013, and references therein).

Finally, it is unclear if it is possible at all to define stability functions for the case of extreme stability (e.g., Grachev et al. 2013) because only very few measurements are available in the range Ri$_b \geq 0.2$–0.25. However, some SHEBA data as well the new data of Srivastava et al. (2020) refer also to this extremely stable range and the G2007a functions are at least within the scatter of data (see also sections 4 and 6).

3. Bulk parameterizations in the framework of MOST

Many atmospheric models use a bulk formulation of the turbulent fluxes based on MOST. Also bulk transfer coefficients can be derived from this theory as follows. One obtains the x (west–east) and y (south–north) components of momentum transport as

$$\tau_x = -\rho C_d |\mathbf{U}(z)|U(z), \quad \tau_y = -\rho C_d |\mathbf{U}(z)|V(z). \tag{15}$$

Here, U and V are the x and y components of the wind vector $\mathbf{U}$, $|\mathbf{U}(z)| = (U^2 + V^2)^{1/2}$ as before. C_d is the transfer coefficient for momentum related to the height z of the lowest model grid level. Similarly, the well known corresponding equation for heat transport H reads

$$H = -\rho c_p C_h |\mathbf{U}(z)|[\Theta_v(z) - \Theta_0], \tag{16}$$

with the transfer coefficient for heat C_h (see also appendix B). Θ_v is the (virtual) potential temperature. Index 0 refers to the surface value. C_d and C_h can be written as

$$C_d = C_{dn}f_m; \quad C_h = C_{hn}f_h, \tag{17}$$

where C_{dn} and C_{hn} are the transfer coefficients for neutral stratification

$$C_{dn} = \frac{\kappa^2}{\ln^2\varepsilon_m}, \quad C_{hn} = \frac{\kappa^2}{\mathrm{Pr}_0 \ln\varepsilon_m \ln\varepsilon_t}. \tag{18}$$

The neutral transfer coefficients depend only on surface properties, and we consider their values as prescribed. In Eq. (17) f_m and f_h are nondimensional functions
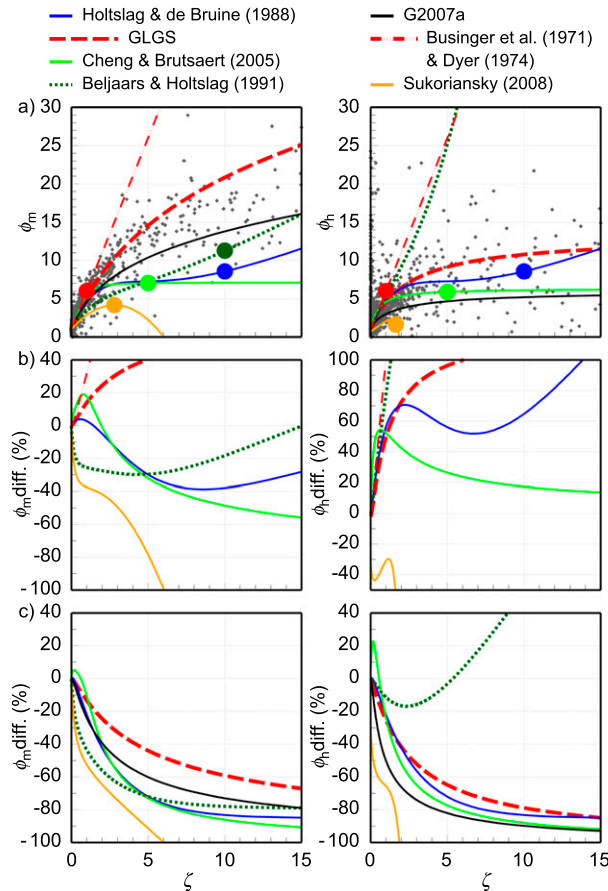
FIG. 1. (a) The stability functions ϕ_m and ϕ_h of Businger et al. (1971) and Dyer (1974), Holtslag and De Bruin (1988), Beljaars and Holtslag (1991), Cheng and Brutsaert (2005), G2007a [Eqs. (24) and (25)], and Sukoriansky (2008), and the functions (32) and (33) (GLGS) plotted vs ζ. Individual 1-h averaged SHEBA data based on median fluxes for five levels are shown as gray symbols. ζ refers here to the local value at the measurement height. Closed circles mark the maximum ζ, for which the functions are defined. The red circle refers to the Businger–Dyer curve. Curves without circle are defined for the whole range shown. Percentage error of ϕ_m and ϕ_h (b) relative to the G2007a functions and (c) relative to the Businger–Dyer functions. The maximum ζ in (b) and (c) are the same as in (a) (not shown).

FIG. 2. (a) As in Fig. 1, but for stability correction functions ψ_m and ψ_h.

depending on both surface properties and stability such that $f_m = f_h = 1$ for neutral conditions. According to Eq. (17) f_m and f_h are considered as drag and heat transfer coefficients normalized by their neutral values. Sometimes, the f_m and f_h functions are also called stability functions, correction functions or mixing functions in the context of numerical modeling (see, e.g., Louis 1979; Louis et al. 1981; Viterbo et al. 1999). We use the term normalized transfer coefficients in the following to avoid confusion with the MOST stability functions ϕ_m and ϕ_h and with the MOST stability correction functions ψ_m and ψ_h.
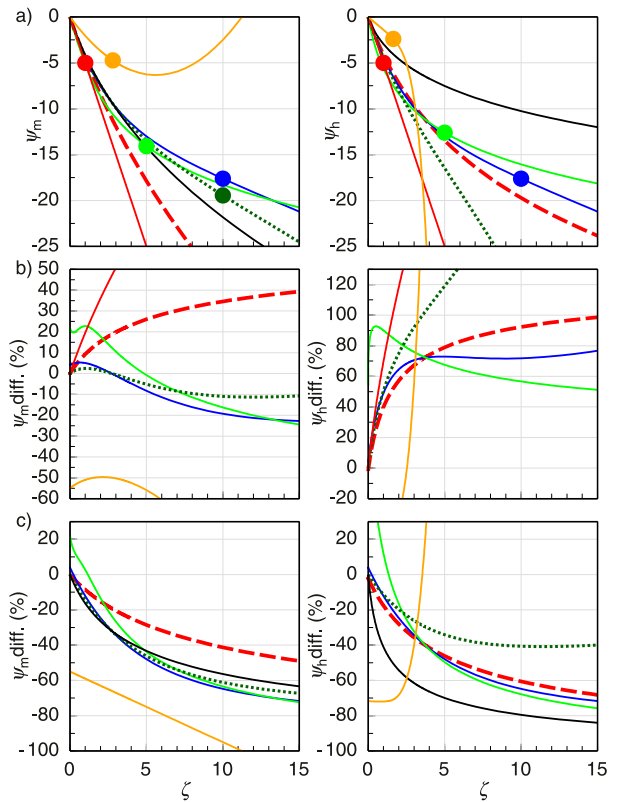
The normalized transfer coefficients f_m and f_h are formulated in agreement with MOST using ψ_m and ψ_h [see definition in textbooks; e.g., Eqs. (3.44) and (3.49) of Garratt (1992)] as

$$f_m = \left[1 - \frac{\psi_m(\zeta) - \psi_m(\zeta/\varepsilon_m)}{\ln \epsilon_m} \right]^{-2}, \tag{19}$$

$$f_h = \left[1 - \frac{\psi_m(\zeta) - \psi_m(\zeta/\varepsilon_m)}{\ln \varepsilon_m} \right]^{-1} \left[1 - \frac{\psi_h(\zeta) - \psi_h(\zeta/\varepsilon_t)}{\mathrm{Pr}_0 \ln \varepsilon_t} \right]^{-1}. \tag{20}$$

The set of bulk MOST equations can be combined to a single equation for the Obukhov length given by

$$\zeta = \mathrm{Ri}_b \frac{1 - 1/\varepsilon_t}{(1 - 1/\varepsilon_m)^2} \frac{[\ln \varepsilon_m - \psi_m(\zeta) + \psi_m(\zeta/\varepsilon_m)]^2}{\mathrm{Pr}_0 \ln \varepsilon_t - \psi_h(\zeta) + \psi_h(\zeta/\varepsilon_t)}. \tag{21}$$

This flux–profile relationship relates the stability correction functions of both momentum and heat to each other, in contrast to the familiar flux–gradient relationships (4) and (5) and flux–profile relationships (9) and (10). The bulk Richardson number Ri_b naturally appears in Eq. (21) as the

main nondimensional parameter. It provides an integral measure of stability in the layer $0 \le z' \le z$ and combines the wind speed U and temperature Θ_v at a level z as

$$\mathrm{Ri}_b = \frac{g}{\Theta} \frac{(\Theta_v - \Theta_s)/(z - z_t)}{U^2/(z - z_0)^2}. \tag{22}$$

Thus, according to the bulk MOST formulation, the set of MOST equations must be solved for fluxes using wind speed U and the temperature difference $\Theta_v - \Theta_s$ as external forcing parameters and considering the roughness length scales for momentum z_0 and heat z_t as given.

Solutions of Eq. (21) express the stability parameter ζ as an implicit, multivariate function of Ri_b, Pr_0, ε_m, and ε_t. When the solution $\zeta = \zeta(\mathrm{Ri}_b, \mathrm{Pr}_0, \varepsilon_m, \varepsilon_t)$ of Eq. (21) is known one can substitute it in the equations specifying the ψ_m and ψ_h functions. We can use, e.g., Eqs. (34) and (35) (see section 6) in Eqs. (19) and (20) to find the normalized transfer coefficients, so also the fluxes of momentum (15) and heat (16).

For practical purposes and without loss of generality, it is convenient to rewrite Eq. (21) in the form

$$\widehat{\mathrm{Ri}}_b = \frac{(1 - 1/\varepsilon_m)^2}{1 - 1/\varepsilon_t} \zeta \frac{\ln\varepsilon_t - \mathrm{Pr}_0^{-1}[\psi_h(\zeta) + \psi_h(\zeta/\varepsilon_t)]}{[\ln\varepsilon_m - \psi_m(\zeta) + \psi_m(\zeta/\varepsilon_m)]^2},$$
$$\widehat{\mathrm{Ri}}_b = \frac{\mathrm{Ri}_b}{\mathrm{Pr}_0}, \tag{23}$$

which is often called the governing MOST equation (see, e.g., Gryanik and Lüpkes 2018). In (23) $\widehat{\mathrm{Ri}}_b$ is the equivalent bulk Richardson number combining Ri_b and Pr_0. We stress that Ri_b and Pr_0 appear in Eq. (21) as the ratio $\widehat{\mathrm{Ri}}_b = \mathrm{Ri}_b/\mathrm{Pr}_0$. Although Pr_0 is occurring on the right-hand side of Eq. (23), it does not really depend on Pr_0^{-1} because its cancellation with Pr_0 occurring in the definition of ψ_h according to Eq. (11) with Eq. (7).

For $\mathrm{Pr}_0 = 1$ the governing MOST Eq. (23) coincides with the corresponding equation, e.g., in Gryanik and Lüpkes (2018).

In general, the solutions of the governing MOST Eq. (23) are provided by an iterative numerical method (see, e.g., Berkowicz and Prahm 1982). The description of many different numerical approaches and arising difficulties is given, e.g., by Jiménez et al. (2012). Approximate analytical solutions are also possible in some cases. They are obtained as a rule by semianalytical methods, see, e.g., Launiainen (1995), discussion of different methods by van den Hurk and Holtslag (1997) and later works by Pleim (2006), Li et al. (2010, 2014), and Gryanik and Lüpkes (2018) to mention a few.

4. Stability functions of G2007a

The main ingredients of MOST are the stability functions $\phi_m(\zeta)$ and $\phi_h(\zeta)$ [see Eqs. (4) and (5)]. For Arctic ocean conditions these functions were derived by G2007a from SHEBA measurements (see introduction). G2007a obtained the best agreement with these data by using

$$\phi_m(\zeta) = 1 + a_m \frac{\zeta(1 + \zeta)^{1/3}}{1 + b_m\zeta}, \quad 0 \le \zeta < 100 \tag{24}$$

and

$$\phi_h(\zeta) = 1 + \frac{a_h\zeta + b_h\zeta^2}{1 + c_h\zeta + \zeta^2}, \quad 0 \le \zeta < 100 \tag{25}$$

with $a_m = 5$, $b_m = a_m/6.5 = 0.77$, $a_h = 5$, $b_h = 5$, and $c_h = 3$. Using then Eqs. (24) and (25) in the first of the Eq. (11) G2007a derived the stability correction functions as

$$\psi_m(\zeta) = -\frac{3a_m}{b_m}\left\{(x - 1) - \frac{B_m}{6}\left[2\ln\frac{x + B_m}{1 + B_m} - \ln\frac{x^2 - xB_m + B_m^2}{1 - B_m + B_m^2}\right.\right.$$
$$\left.\left. -2\sqrt{3}\left(\arctan\frac{2x - B_m}{\sqrt{3}B_m} - \arctan\frac{2 - B_m}{\sqrt{3}B_m}\right)\right]\right\} \tag{26}$$

and

$$\psi_h(\zeta) = -\left(\frac{a_h}{B_h} - \frac{b_hc_h}{2B_h}\right)\left(\ln\frac{2\zeta + c_h - B_h}{2\zeta + c_h + B_h} - \ln\frac{c_h - B_h}{c_h + B_h}\right)$$
$$-\frac{b_h}{2}\ln(1 + c_h\zeta + \zeta^2), \tag{27}$$

where $x = (1 + \zeta)^{1/3}$, $B_m = (1/b_m - 1)^{1/3} > 0$, and $B_h = (c_h^2 - 4)^{1/2}$. The region of applicability for ψ_m and ψ_h is the same as for ϕ_m and ϕ_h.

The stability functions (24) and (25) are shown in Fig. 1a and in Fig. 3a together with the corresponding SHEBA data and with the data of Srivastava et al. (2020),
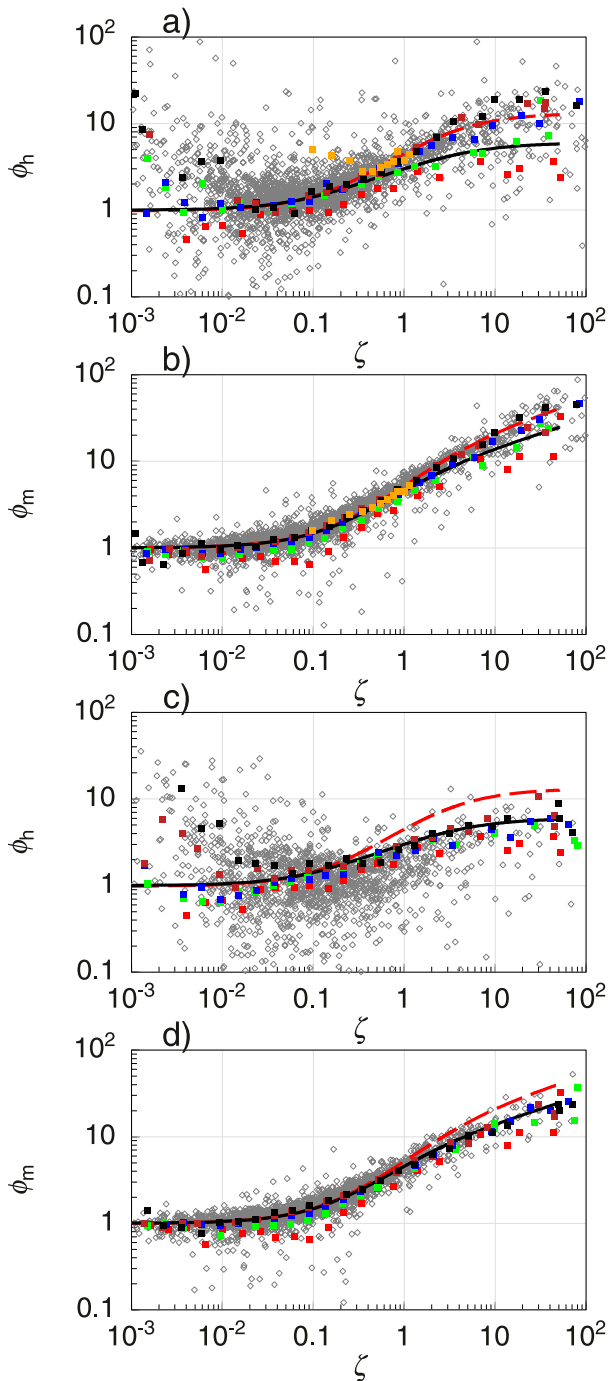
FIG. 3. Stability functions (a),(c) ϕ_h and (b),(d) ϕ_m as a function of ζ (log–log scaling). Gray symbols represent SHEBA 1-h averaged data based on the median fluxes for five measurement levels. In (a) and (b) $\zeta = z_n/L_1$, where L_1 is the Obukhov length at the lowest measurement level $n = 1$ and in (c) and (d) $\zeta = z_n/L_1$, where L is the local Obukhov length and n is the level number. Squares represent bin-averaged data at the measurement levels (red: 2.2 m; green: 3.2 m; blue: 5.1 m; brown: 8.9 m; black: 14–18.2 m; all SHEBA) and orange squares are the Ranchi data (Srivastava et al. 2020) obtained at 10 m height. The black solid line represents

which will be called in the following the Ranchi data. The selection of these data shown here represent the most accurate ones (those filtered with $\mathrm{Ri}_f < 0.25$, where Ri_f is the flux Richardson number, value for $\zeta = 0.05$ is not included here) (see Srivastava et al. 2020). Ranchi data without this filtering are for $\zeta > 1.2$ very close to the data observed during SHEBA at 2.2 m height (red squares) (not shown). As all other MOST stability functions the G2007a functions are affected by self-correlation features since they are traditionally defined via variables (e.g., friction velocity or temperature) occurring also in the arguments of these functions due to the Obukhov length. But, as shown by the analysis of Grachev et al. (2013, 2015) of the SHEBA data, self-correlation has a reasonably small effect.

The functional forms of ϕ_m and ϕ_h were designed using the following physical and practical constraints:

(i) The functions have the correct linear dependence on ζ at small $\zeta \to 0$, namely, $\phi_m \approx 1 + a_m\zeta$ and $\phi_h \approx 1 + a_h\zeta$. For large ζ, the u_*-less (frictionless scaling) limit holds (see G2007a for a discussion), i.e., the function ϕ_m is proportional to $(a_m/b_m)\zeta^{1/3}$ for $\zeta \to \infty$. The function ϕ_h approaches a constant value $\phi_h = 1 + b_h$ in the limit $\zeta \to \infty$. This characteristic, which does not follow the z-less scaling approach has been discussed in detail by G2007a. A consequence is that the nonneutral Prandtl number $\mathrm{Pr} = \phi_m/\phi_h$ is approaching zero at $\zeta \to \infty$, which is not in line with theories (e.g., Nieuwstadt 1984) but in good agreement with the SHEBA data [see discussion of the Prandtl number in Grachev et al. (2007b), and their Fig. 1c]. In such strongly stable conditions, frictional effects become small or even negligible and the surface friction velocity associated with the mean flow may no longer be a dominant governing velocity scale. For example, in this regime, the influence of the Coriolis effect and gravity waves comes into play. In particular, in the limit of very strong stability, decaying stress becomes comparable to the Coriolis force even near the surface leading to significant rotation of the wind vector with height (Ekman spiral) (Grachev et al. 2008). Also, it can be shown that when Eqs. (32) and (33) are used, u_* has still some impact in the practically most relevant stability range ($\zeta < 100$), and that Pr is still far from zero at $\zeta \to 100$.

←

the functions of G2007a, the red dashed line shows the new functions (32) and (33) using the optimal coefficients (38) $\mathrm{Pr}_0 = 0.98$ and $a_m = 5.0$, $b_m = 0.3$, $a_h = 5.0$, and $b_h = 0.4$.

(ii) Stability functions fit the SHEBA data in the entire range of available ζ reasonably well.

(iii) The functions $\phi_m(\zeta)$ and $\phi_h(\zeta)$ should be analytically integrable functions of ζ, resulting in analytical stability correction functions $\psi_m(\zeta)$ and $\psi_h(\zeta)$.

One should also pay attention to the fact that the $\phi_h(\zeta)$ function of G2007a suggest $Pr_0 = 1$. Actually, it is an additional constraint, which is implicitly imposed by constraint (i).

The functions by G2007a have been shown to be valid in a large range of stabilities (see section 1). In this connection it is important to mention the discussion presented in Grachev et al. (2013) showing that the strict applicability of MOST is limited to $Ri < Ri_{cr} \approx 0.2 - 0.25$, where Ri is the gradient Richardson number and index cr refers to the critical value. That is, the applicability limit for ϕ_m and ϕ_h is $Ri < Ri_{cr}$. However, for practical purposes (model parameterizations) we are forced to use ϕ_m and ϕ_h in the supercritical regime (beyond its strict limit of applicability). $Ri \approx Ri_{cr}$ corresponds to $\zeta \approx 1$ but practically we need parameterizations for $\zeta \gg 1$, maybe up to $\zeta \approx 100$ and higher. The application of MOST for $\zeta \gg 1$ is common practice in the modeling community. Note, that according to Grachev et al. (2013) (Figs. 7 and 8), the upper limit of MOST in the SBL coincides with the region, for which the Kolmogorov power law is applicable. In other words, the condition $Ri \approx Ri_{cr}$ also separates Kolmogorov and non-Kolmogorov turbulence in stratified turbulent shear flows.

Nevertheless, the G2007a functions agree well with the SHEBA measurements in the given range up to $\zeta = 100$ and in the range of scatter with functions of other authors mentioned in section 2 (thus with data obtained over land) for the less stable conditions (see G2007a). Figure 1b visualizes the differences between the functions (24) and (25) and other ones relative to the functions of G2007a. The latter agree well with the other functions in the region of near-neutral and weak stability as emphasized more clearly in Fig. 1c, where differences relative to Businger–Dyer functions are shown. On the contrary, in the region of very stable and extremely stable conditions the differences between all stability functions are large.

According to G2007a the stability functions of Businger–Dyer are applicable up to $\zeta \approx 1$, of Chenge and Brutsaert (2005) up to $\zeta \approx 5$ and of Holtslag and De Bruin (1988) and Beljaars and Holtslag (1991) for $\zeta < 10$. The functions of G2007a are, however, well supported by measurements for $1 < \zeta < 100$. As shown in Figs. 1 and 2, the scatter of functions [see Eqs. (4) and

(5) for definition] is smaller in their confidence ranges than beyond these ranges.

The differences are also well pronounced in the stability correction functions ψ_m and ψ_h. This can be seen in Fig. 2 showing results for functions of all authors mentioned so far.

5. Stability parameter ζ and transfer coefficients based on stability functions of G2007a

When stability functions are derived the next logical step is to check the performance of the functions for the representation of bulk transfer coefficients since the latter are the main ingredients of surface-layer schemes in weather prediction and climate models. This requires (see section 3) the calculation of the stability parameter ζ as a function of Ri_b, ε, ε_t, and Pr_0 following the governing MOST Eq. (21).

In Figs. 4a and 4b we show ζ obtained from the SHEBA data together with ζ derived by Gryanik and Lüpkes (2018) with Eq. (21) using the stability correction functions (26) and (27). The latter results are included for a wide range of the roughness parameters ε and ε_t. In agreement with Fairall and Markson (1987), Hartmann et al. (1994), G2007a, Andreas et al. (2010a,b), Lüpkes et al. (2012), Castellani et al. (2014), and with the summary by Gryanik and Lüpkes (2018) the most often found range of stability is $0 \leq Ri_b \leq 0.2$ and the most representative ranges of the surface roughnesses are

$$2 \times 10^2 \leq \varepsilon_m \leq 1.4 \times 10^6, \quad \varepsilon_m \leq \varepsilon_t \leq 10^2 \varepsilon_m, \quad (28)$$

which corresponds to roughness lengths

$$7.1 \times 10^{-6} \leq z_0 \leq 5 \times 10^{-2} \text{ m}, \quad 10^{-2} z_0 \leq z_t \leq z_0 \quad (29)$$

and to neutral drag coefficients at 10 m height

$$0.8 \times 10^{-3} \leq C_{dn} \leq 5.7 \times 10^{-3}. \quad (30)$$

In rare cases values are outside of this range, e.g., even $\varepsilon > 1 \times 10^{12}$ (or $C_{dn} < 0.2 \times 10^{-3}$) has been reported by Elvidge et al. (2016). However, we consider the values

$$\begin{aligned} \varepsilon_m &= 3 \times 10^4 \quad \text{and} \quad \varepsilon_t = 1.5 \times 10^5, \\ C_{dn} &= 1.5 \times 10^{-3} \quad \text{and} \quad C_h = 1.3 \times 10^{-3} \end{aligned} \quad (31)$$

as the most typical ones. They are calculated with $z = 10$ m, $z_0 = 3.3 \times 10^{-4}$ m, and $\alpha = z_t/z_0 = 0.2$.

The most unexpected finding from Fig. 4 is that $\zeta(Ri_b)$ obtained from Eq. (21) with Eqs. (26) and (27) overestimates the measured ζ by far (note the logarithmic ζ axis) in the range of small Ri_b ($Ri_b < 5 \times 10^{-2}$) when the most typical roughness conditions over sea ice [Eq. (31)]
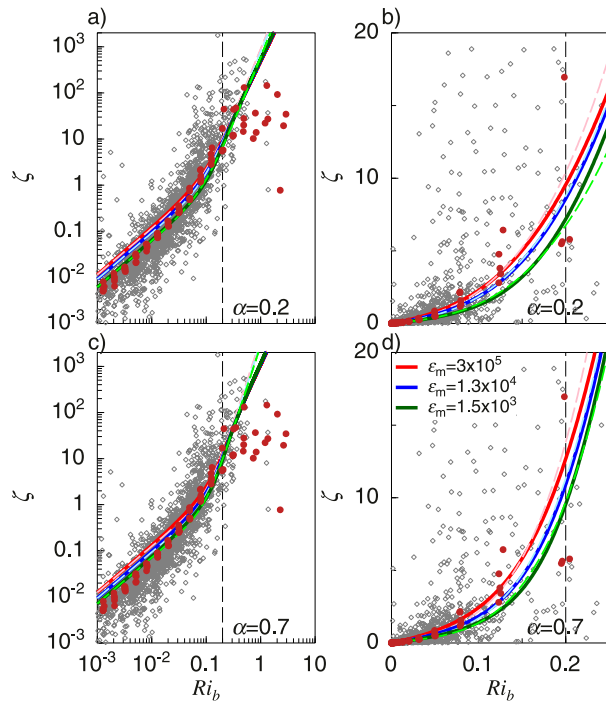
FIG. 4. Stability parameter ζ as a function of Ri_b. (a),(b) The red, blue, and green solid lines are results obtained with the G2007a functions while the dashed lines represent the corresponding parameterizations of Gryanik and Lüpkes (2018). The blue line belongs to the mean roughness of sea ice found during SHEBA (called here most typical roughness). Other colored lines belong to extremely low (red) and large (green) roughness. Gray symbols represent SHEBA 1-h averaged data based on the median fluxes for five measurement levels. Brown bullets represent bin-averaged SHEBA observations. (c),(d) As in (a) and (b), but colored solid lines were obtained with the new stability correction functions (34) and (35) using the optimal coefficients (38) $Pr_0 = 0.98$ and $a_m = 5.0$, $b_m = 0.3$, $a_h = 5.0$, and $b_h = 0.4$. Dashed lines represent the approximate solution as explained in section 8.

are prescribed. In the range around $Ri_b = 0.2$ there is an underestimation compared with the measurements.

This finding is crucial since it has a tremendous impact on the parameterization of turbulent fluxes of momentum and heat. Indeed, panels a and b of Figs. 5 and 6 show that for the typical roughness regime [Eq. (31)] there are drawbacks with respect to C_d and especially for C_h. Results obtained for C_h with the G2007a stability correction functions tend to underestimate the observations for $Ri_b < 0.02$ and both C_d and C_h overestimate the observations for $Ri_b > 0.05$ (see also Fig. D5). This means that using the G2007a functions would cause also an under/overestimation of the momentum and heat fluxes in the corresponding stability ranges. Choosing a larger surface roughness would improve fluxes for near-neutral conditions but would result in an even stronger overestimation for the very stable and extremely stable ranges.
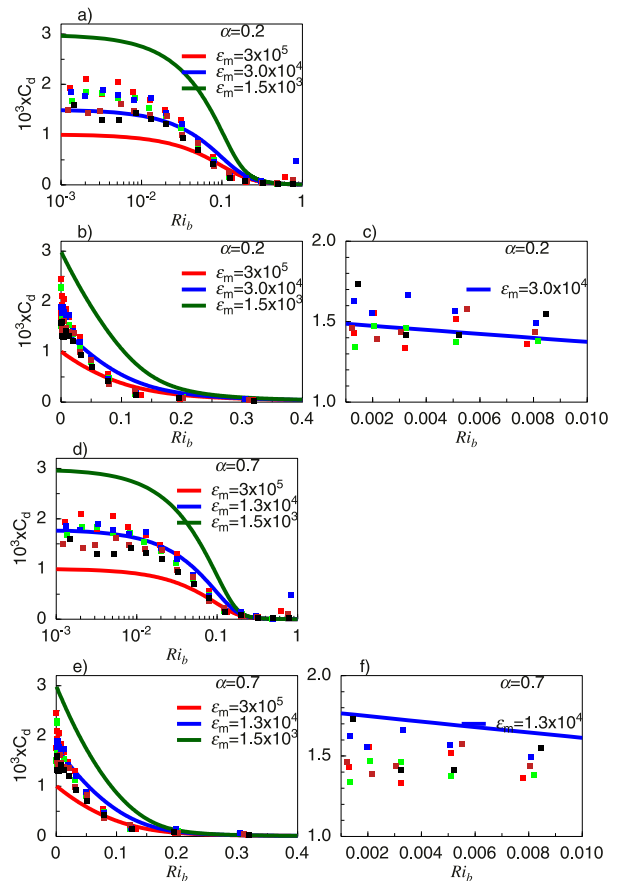

FIG. 5. Transfer coefficients C_d as functions of Ri_b. The red, blue, and green solid lines represent the parameterizations of C_d and C_h for $z_{10} = 10$ m height of Gryanik and Lüpkes (2018) (a)–(c) based on the stability functions of G2007a and (d)–(f) based on the GLGS functions. The blue lines in (a)–(c) and (d)–(f) represent the range of "typical" roughness of sea ice but note that different ε_m and α values were used. The other colored lines belong to extremely low (red) and large (green) roughness. Colored squares in (a), (b), (d), and (e) are the SHEBA observations at the measurement heights $z = 2.2$ (red), 3.2 (green), 5.0 (blue), 8.9 (brown), and 14–18 m (black). In (c) and (f) the squares represent the measurements but related to z_{10} applying the formula $C_{dn10} = [\log(z/z_0)/\log(z_{10}/z_0)]^2 C_{dn}$ with $z_0 = 2 \times 10^{-4}$ m.

The results described above motivate us to search for new stability functions, which are suited to find a compromise, i.e., they should represent the local gradients from one side, the $\zeta(Ri_b)$ dependence and the bulk transfer coefficients $C_d(Ri_b)$ and $C_h(Ri_b)$ from the other side, but all with reasonable accuracy.

6. New modified and extended stability functions

To overcome the drawbacks described in the previous section we suggest here new stability functions for sea ice–covered polar regions. They are—as the G2007a
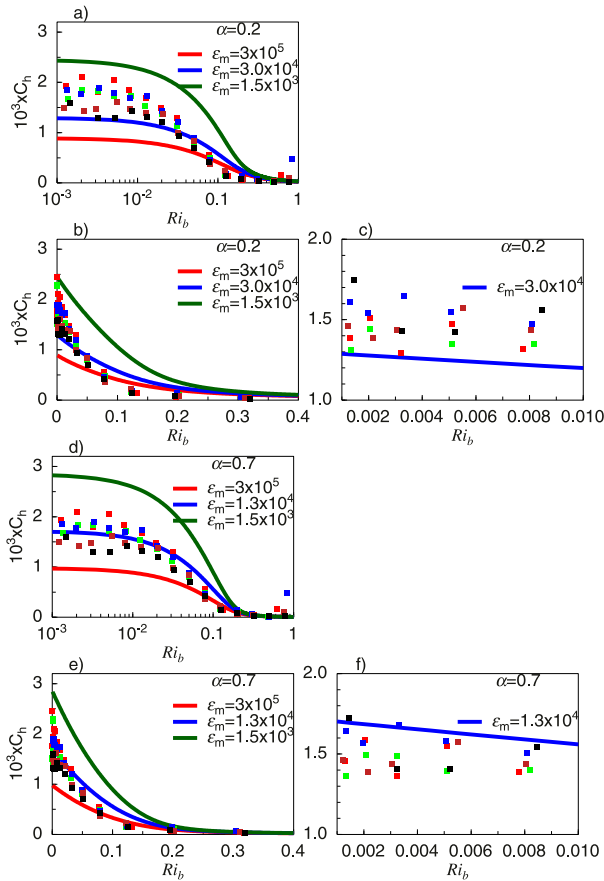
FIG. 6. As in Fig. 5, but for C_h and values related to $z_{10} = 10$ m height are obtained assuming that $C_{hn10} = [\log(z/z_0)/\log(z_{10}/z_0)][\log(z/z_t)/\log(z_{10}/z_t)]C_{hn}$ with $z_t = 1.4 \times 10^{-4}$ and $z_0 = 2 \times 10^{-4}$ m.

functions—also based on the SHEBA data and on theoretical arguments but—as will be shown—they are less complex than the G2007a functions and they slightly better represent the relationships between fluxes and the nondimensional gradients $\phi_m = \phi_m(\zeta)$, and $\phi_h = \phi_h(\zeta)$, and between the stability parameter and the bulk Richardson number $\zeta = \zeta(\mathrm{Ri}_b)$. Most important is that the application of the new functions improve also the relationship between bulk transfer coefficients and bulk Richardson numbers $C_d = C_d(\mathrm{Ri}_b)$ and $C_h = C_h(\mathrm{Ri}_b)$.

In the following, we first propose the new stability functions. Then, we optimize free constants of these functions in order to improve the representation of the observed relationships.

a. Functional form of new stability functions

We suggest modified universal stability functions as

$$\phi_m(\zeta) = 1 + \frac{a_m \zeta}{(1 + b_m \zeta)^{2/3}}, \qquad 0 \le \zeta < 100, \qquad (32)$$

$$\phi_h(\zeta) = \mathrm{Pr}_0\left(1 + \frac{a_h \zeta}{1 + b_h \zeta}\right), \qquad 0 \le \zeta < 100, \qquad (33)$$

where a_m, b_m, a_h, and b_h are empirical constants (their values will be determined in the next section), and Pr_0 is the neutral-limit Prandtl number as before.

These functions are very similar to those suggested by G2007a [cf. Eqs. (32) and (33) with Eqs. (24) and (25)]. But they are defined by only four empirical constants and lead to arithmetically simple modified stability correction functions. After integration of Eqs. (32) and (33) we find

$$\psi_m(\zeta) = -3\frac{a_m}{b_m}[(1 + b_m\zeta)^{1/3} - 1], \quad 0 \le \zeta < 100, \quad (34)$$

$$\psi_h(\zeta) = -\mathrm{Pr}_0\frac{a_h}{b_h}\ln(1 + b_h\zeta), \quad 0 \le \zeta < 100. \qquad (35)$$

It is important to emphasize that the constraints (i) to (iii) (see section 4) formulated by G2007a do not define stability functions uniquely (see the discussion by G2007a), and that all the constraints are satisfied by the modified functions (32) and (33) as well. In particular, the limits of the new stability function (32) and (33) for $\zeta \to 0$ and $\zeta \to \infty$ are similar to those of the G2007a functions. The asymptotes are given as

$$\phi_m(\zeta) = \begin{cases} 1 + a_m\zeta, & \zeta \to 0, \\ (a_m/b_m^{2/3})\zeta^{1/3}, & \zeta \to \infty \end{cases} \qquad (36)$$

and

$$\phi_h(\zeta) = \mathrm{Pr}_0 \begin{cases} 1 + a_h\zeta, & \zeta \to 0, \\ 1 + a_h/b_h, & \zeta \to \infty. \end{cases} \qquad (37)$$

Correspondingly, the asymptotes of the new stability correction functions (34) and (35) are similar to those of the G2007a functions. In the following, we call the new modified stability functions (32) and (33) and new stability correction functions (34) and (35) GLGS functions for simplicity.

b. Optimization of empirical constants of new stability functions

To improve the representation of the observed relationships we apply a new optimization strategy for the GLGS functions, which has not been applied until now: Keeping their functional form unchanged, we assume that the constants a_m, a_h, b_m, and b_h should not be obtained by optimizing either the agreement with the observed $\phi_m = \phi_m(\zeta)$ and $\phi_h = \phi_h(\zeta)$ or with the observed $\zeta = \zeta(\mathrm{Ri}_b)$, $C_d = C_d(\mathrm{Ri}_b)$, and $C_h = C_h(\mathrm{Ri}_b)$ independently from each other, but by the best fit of the functions altogether.

The optimization of the coefficients depends on the ranges of the parameters ε and ε_t and on the value of Pr_0.

For $\varepsilon, \varepsilon_t$ we consider the ranges (28). There is no obvious reason to use another value than $\mathrm{Pr}_0 = 1$ (see G2007a) or $\mathrm{Pr}_0 = 0.98$ (see Sorbjan and Grachev 2010; Sorbjan 2017) as the most relevant value for the SHEBA data.

Applying the trial and error method we find as a compromise the optimal constants

$$\mathrm{Pr}_0 = 0.98, \quad a_m = 5.0, \quad a_h = 5.0, \quad b_m = 0.3, \quad b_h = 0.4, \tag{38}$$

which result in stability functions well suited to represent all relationships mentioned above simultaneously.

The optimized stability functions ϕ_m and ϕ_h and the stability correction functions ψ_m and ψ_h are shown in Figs. 1 and 3 partly together with SHEBA data and with the functions of G2007a. The corresponding approximation of the stability parameter $\zeta(\mathrm{Ri}_b)$ is shown in Figs. 4c and 4d. The transfer coefficients C_d and C_h based on the new functions are given in Figs. 5d–f and 6d–f.

One can see from Figs. 1 and 3 that the GLGS functions (32) and (33) with the constants (38) fit the SHEBA data reasonably well especially when the locally measured fluxes are used (Figs. 3a,b). Compared with the G2007a functions there is an improvement in the range $\zeta > 5$ for the local data (especially upper-level measurements between 5 and 18 m height). The modified ϕ_h function agrees also slightly better with the Ranchi data than the G2007a function in the shown range. Also, a slight improvement of agreement with the SHEBA data relative to the G2007a functions is found for the $\zeta(\mathrm{Ri}_b)$ relationship for $0.15 < \zeta < 0.25$ (see Figs. 4b,d). There is also some improvement for $\mathrm{Ri}_b < 0.02$ (see Figs. 4a and 4c with logarithmic x axes). Namely, for $\mathrm{Ri}_b < 0.02$ the blue curve for the typical conditions is slightly closer to the observations when the modified functions are chosen. Note that we used here the values

$$\varepsilon = 1.3 \times 10^4, \quad \varepsilon_t = 1.86 \times 10^4 \tag{39}$$

instead of those given by Eq. (31). The corresponding values in terms of transfer coefficients at 10 m height and roughness lengths are

$$C_{dn} = 1.78 \times 10^{-3}, \quad C_{hn} = 1.72 \times 10^{-3},$$

$$z_0 = 7.7 \times 10^{-4} \, \mathrm{m}, \quad z_t = 5.4 \times 10^{-4} \, \mathrm{m}, \tag{40}$$

so that $\alpha = z_t/z_0 = 0.7$. This modification results from the demand to improve the $\zeta(\mathrm{Ri}_b)$ relation in the near-neutral range where the sensitivity to the roughness is large (see Fig. 4). The new values, which we call in the following also "typical," represent a compromise since in the near-neutral range values of C_d and C_h are at the

upper limit of the bin averaged SHEBA observations (Figs. 5 and 6, panels d–f). Finally, there is also an improvement for the transfer coefficients $C_d(\mathrm{Ri}_b)$ and $C_h(\mathrm{Ri}_b)$ especially in the range $\mathrm{Ri}_b < 0.01$ (Figs. 5, 6) but also in the range $\mathrm{Ri}_b > 0.1$ (Fig. D5), which is most important since the transfer coefficients determine the fluxes. This is further discussed in section 11 and appendix D.

We stress that the GLGS functions should be understood as a replacement of the G2007a functions for two reasons. The first is the improvement with respect to measurements. Here, especially, the improvement resulting for the transfer coefficients is important since they influence the fluxes. The second is that the new functions allow a more efficient use of the G2007a findings. In general, they are more suitable for the solution of particular problems as will be argued in the following sections discussing benefits of using the new stability functions.

Moreover, it is important to note that according to our analysis the best fit of the new functions either to the stability functions by G2007a or to a version with optimal agreement between the parameterized and the observed $\zeta(\mathrm{Ri}_b)$ relationship results in significantly different fitting constants. Optimal coefficients Pr_0, a_m, b_m, a_h and b_h for these both limiting cases are provided in appendix D. The constants (38) are optimal for the full ranges (28). It is obvious that the reliability of the coefficients depends on the ranges of ζ and Ri_b, for which the functions are defined. A better agreement can be reached, e.g., when the range is limited to $0.05 < \zeta \leq 10$. We will discuss this issue also in appendix D.

7. Benefits of using the GLGS functions

A numerically efficient calculation of turbulent fluxes for momentum and heat in weather prediction and climate models requires analytically simple formulations of functions representing the wind and temperature profiles.

It is obvious that the new simple functional form of the stability functions (34) and (35) is an advantage and a necessary prerequisite for obtaining an approximate analytical solution of the nonlinear governing MOST Eq. (23). Using the simpler GLGS functions in the governing MOST equation, a solution $\zeta = \zeta(\mathrm{Ri}_b, \varepsilon_m, \varepsilon_t)$ can be found more easily. It can be used to obtain new parameterizations of the transfer coefficients $C_d = C_d(\mathrm{Ri}_b, \varepsilon_m, \varepsilon_t)$ and $C_h = C_h(\mathrm{Ri}_b, \varepsilon_m, \varepsilon_t)$ and finally of the unknown turbulent fluxes τ and H. It can be expected that these parameterizations are analytically simpler than the solution of Gryanik and Lüpkes (2018), which is based on the original stability correction functions of G2007a, so that it can be installed with less programming effort in numerical models. It is also expected that the

parameterizations would be more accurate because the empirical relationships $\zeta = \zeta(\mathrm{Ri}_b)$, $C_d = C_d(\mathrm{Ri}_b)$, and $C_h = C_h(\mathrm{Ri}_b)$ were already taken into account while constructing the new stability functions.

Many other advantages of using simple analytical formulations for stability functions are discussed by Pleim (2006) and Lüpkes et al. (2012). For example, the normalized transfer coefficients f_m and f_h are the main ingredients of mixing-length closure schemes (also often called first-order closure models or K theory) used in the atmospheric boundary layer in many climate models. According to the hypothesis of Louis (1979) these functions characterize the stability effects on eddy viscosity K_m and on the eddy scalar diffusion coefficient K_h with

$$K_m = -\frac{\overline{w'u'}}{\partial U/\partial z} = l_m^2 f_m \left|\frac{d\mathbf{U}}{dz}\right|, \quad K_h = -\frac{\overline{w'\theta'}}{\partial \Theta/\partial z} = l_m l_h f_h \left|\frac{\partial \Theta}{\partial z}\right|,$$
(41)

when the bulk Richardson number is replaced by its numerical gradient Richardson number counterpart. Here, U and V are the x and y components of the mean wind vector $\mathbf{U}$, $|d\mathbf{U}/dz| = [(dU/dz)^2 + (dV/dz)^2]^{1/2}$, $f_m = 1/\phi_m^2$, $f_h = 1/(\phi_m \phi_h)$, and l_m and l_h are the neutral-limit mixing lengths for momentum and temperature, respectively. The simple functional form of the GLGS functions results in the simple Eq. (41).

Another benefit of the GLGS functions, also related to their simplicity, arises when they are used for studying the stability dependence of form drag (Lüpkes and Gryanik 2015). However, both K theory and the effect of form drag are beyond the scope of our current research whose focus is on the parameterization of the near-surface bulk momentum and heat fluxes and corresponding transfer coefficients.

Finally, the new functions result in the observed dependence of the heat flux as a function of ζ with one maximum (not shown here). As shown by Srivastava and Sharan (2019) some other nonlinear stability functions produce two maxima, which contradicts observations.

8. Approximate solution of the governing MOST equation

To solve the governing MOST Eq. (23) using the GLGS functions (34) and (35) we apply a semianalytical approach following Gryanik and Lüpkes (2018).

We search for an approximate solution $\zeta = \zeta(\widehat{\mathrm{Ri}}_b, \varepsilon_m, \varepsilon_t)$ of Eq. (23) in the functional form

$$\zeta = C\widehat{\mathrm{Ri}}_b + A\widehat{\mathrm{Ri}}_b^{\gamma},$$
(42)

with the exponent γ and with the two functions $C(\varepsilon_m, \varepsilon_t)$ and $A(\varepsilon_m, \varepsilon_t, \gamma)$.

The coefficient

$$C = \frac{\ln^2 \varepsilon_m}{\ln \varepsilon_t}$$
(43)

describes the limit $\widehat{\mathrm{Ri}}_b \to 0$. In this limit the first term in Eq. (42) coincides with the exact solution. The coefficients $A(\varepsilon_m, \varepsilon_t, \gamma)$ describe the growth rate of ζ at large $\widehat{\mathrm{Ri}}_b$. As shown by Gryanik and Lüpkes (2018) the coefficient $A(\varepsilon_m, \varepsilon_t, \gamma)$ is given by

$$A = \zeta_a \widehat{\mathrm{Ri}}_{b,a}^{-\gamma} - \frac{\ln^2 \varepsilon_m}{\ln \varepsilon_t} \widehat{\mathrm{Ri}}_{b,a}^{1-\gamma},$$
(44)

with

$$\widehat{\mathrm{Ri}}_{ba} = \frac{(1 - 1/\varepsilon_m)^2}{1 - 1/\varepsilon_t} \zeta_a \frac{\ln \varepsilon_t - \psi_{ha}}{(\ln \varepsilon_m - \psi_{ma})^2},$$
(45)

where

$$\psi_{ma} = \psi_m(\zeta_a) - \psi_m(\zeta_a/\varepsilon_m), \quad \psi_{ha} = \psi_h(\zeta_a) - \psi_h(\zeta_a/\varepsilon_t).$$
(46)

In Eq. (46) ζ_a is the representative value of ζ, for which the function (42) coincides with the exact solution of the governing MOST Eq. (23).

For relevant ranges of $\widehat{\mathrm{Ri}}_b$, ε_m, and ε_t, the optimal values of the two fitting parameters γ and ζ_a are calculated numerically by a variational method using the least squares fit metric

$$J = \frac{1}{\Delta} \int_0^{\widehat{\mathrm{Ri}}_{b,\max}} \int_{\ln \varepsilon_-}^{\ln \varepsilon_+} \int_{\ln \varepsilon_{t-}}^{\ln \varepsilon_{t+}} \left[\frac{f_k(\widehat{\mathrm{Ri}}_b, \varepsilon_m, \varepsilon_t) - f_{k,ex}(\widehat{\mathrm{Ri}}_b, \varepsilon_m, \varepsilon_t)}{f_{k,ex}(\widehat{\mathrm{Ri}}_b, \varepsilon_m, \varepsilon_t)}\right]^2$$
$$\times d\ln \varepsilon_t \, d\ln \varepsilon_m \, d\widehat{\mathrm{Ri}}_b,$$
(47)

where $\Delta = \widehat{\mathrm{Ri}}_{b,\max} \ln(\varepsilon_+/\varepsilon_-)\ln(\varepsilon_{t,+}/\varepsilon_{t,-})$ is a normalization factor. Subscript $k = m$ is used for momentum and $k = h$ for heat. The cost function (47) provides a measure of the deviation of the approximate analytical solution from the exact numerical solution. Note that in Gryanik and Lüpkes (2018) the difference in ζ has been minimized but we take here f_m since finally this is most important for the fluxes. The metric J depends on the two variables γ and ζ_a and on the parameters $\widehat{\mathrm{Ri}}_{b,\max}$, ε_-, ε_+, $\varepsilon_{t,-}$, and $\varepsilon_{t,+}$, which specify the relevant confidence ranges for stability $\widehat{\mathrm{Ri}}_b$ and roughnesses ε_m and ε_t. Values are $\widehat{\mathrm{Ri}}_{b,\max} = 0.3$, and for ε_-, ε_+, ε_{t-}, and ε_{t+} those defined by Eq. (28). We found that minimizing f_m or f_h resulted in values of γ and ζ_a that differed only very slightly from each other.

It is worth to note that the coefficient A can be written in more compact form by combining Eqs. (44)–(46). The result is

$$A = \frac{(\ln\varepsilon_m - \psi_{ma})^{2(\gamma-1)}}{\zeta_a^{\gamma-1}(\ln\varepsilon_t - \psi_{ha})^{(\gamma-1)}}\left[\frac{(\ln\varepsilon_m - \psi_{ma})^2}{\ln\varepsilon_t - \psi_{ha}} - \frac{\ln^2\varepsilon_m}{\ln\varepsilon_t}\right]. \tag{48}$$

Formally, the approximate solution (42) is valid for arbitrary stability functions. However, for given $\psi_m(\zeta)$ and $\psi_h(\zeta)$ the quality of approximation depends on the choice of the particular values of γ and ζ_a. These depend on the specific features of the functional form of the stability functions and on the range of independent variables, i.e., $\widehat{\mathrm{Ri}}_{b,\max}$, ε_-, ε_+, $\varepsilon_{t,-}$, and $\varepsilon_{t,+}$.

Using the GLGS functions (34) and (35) and applying the cost function (47) in the ranges (28) we find the optimal value of the exponent γ and the optimal stability parameter ζ_a for the set of parameters (38) as

$$\gamma = 3.625, \quad \zeta_a = 7.25. \tag{49}$$

Figure 7 shows that the solution (49) is unique. This was similar also for the other parameter sets discussed in section 11.

Inserting values (49) into the general Eqs. (42) and (48) with Eq. (46), one obtains the new parameterization as

$$\zeta = C\widehat{\mathrm{Ri}}_b + A\widehat{\mathrm{Ri}}_b^{3.625}, \tag{50}$$

with the coefficient C given by Eq. (43) and with

$$A = \frac{(\ln\varepsilon_m - \psi_{ma})^{5.25}}{181.3(\ln\varepsilon_t - \psi_{ha})^{2.625}}\left[\frac{(\ln\varepsilon_m - \psi_{ma})^2}{\ln\varepsilon_t - \psi_{ha}} - \frac{\ln^2\varepsilon_m}{\ln\varepsilon_t}\right], \tag{51}$$

where

$$\psi_{ma} = -50.0[1.47 - (1 + 2.17/\varepsilon_m)^{1/3}], \tag{52}$$

$$\psi_{ha} = -12.25\ln[3.9/(1 + 2.9/\varepsilon_t)]. \tag{53}$$

The results obtained by the approximate analytical and exact numerical solutions for the stability parameter ζ are shown in Fig. 8. The curves visualizing the exact solution were obtained numerically by calculating $\widehat{\mathrm{Ri}}_b = \widehat{\mathrm{Ri}}_b(\zeta, \varepsilon_m, \varepsilon_t)$ using Eq. (23) in a given range of ζ for prescribed values of ε_m and ε_t, and then plotting the result $\zeta = \zeta(\widehat{\mathrm{Ri}}_b, \varepsilon_m, \varepsilon_t)$.

Note that in a weather prediction or climate model $\widehat{\mathrm{Ri}}_b$ can be calculated based on the predicted wind and temperature as well as humidity at the surface and
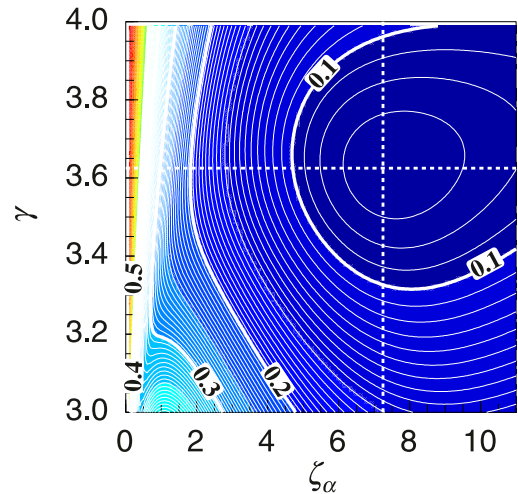

FIG. 7. Cost function J [Eq. (47)] as a function of ζ_a and γ. White dashed lines represent the ideal values (49) with the smallest value of J for the parameter set (38).

first grid level. The most accurate procedure for the necessary determination of $\zeta(\widehat{\mathrm{Ri}}_b)$ is to solve Eq. (23) by numerical iteration. The approximate solution can be calculated, however, by the explicit Eq. (50). It reproduces the exact numerical solution with a mean error smaller than 5% and with a maximal error of 10% in the range $0 < \mathrm{Ri}_b < 0.2$ (so that $0 < \widehat{\mathrm{Ri}}_b < 0.16 - 0.2$ for Pr_0 in the range 0.75–1). The good agreement of the stability parameters obtained from both solutions indicates that our approximation is reasonable for the considered ranges of stability and roughness.

However, the parameterization can be further simplified. For the representative SHEBA values of the roughness parameters, we obtain $\varepsilon_m \gg 1$ and $\varepsilon_t \gg 1$; if so, the small terms $1/\varepsilon_m$, $1/\varepsilon_t$ and $\psi_m(\zeta_a/\varepsilon_m)$ and $\psi_m(\zeta_a/\varepsilon_m)$ in Eqs. (45) and (46) can be neglected. Then the functions ψ_{ma} and ψ_{ha} in Eqs. (52) and (53) become independent on the roughness parameters and can be replaced by the constant values $\psi_{ma} = -23.50$ and $\psi_{ha} = -16.67$. As a result of all these simplifications, the parameterization of the stability parameter ζ is provided by Eq. (50) with the coefficient C as before and with the simplified coefficient (51) found as

$$A = \frac{(\ln\varepsilon_m + 23.50)^{5.25}}{181.3(\ln\varepsilon_t + 16.67)^{2.625}}\left[\frac{(\ln\varepsilon_m + 23.50)^2}{\ln\varepsilon_t + 16.67} - \frac{\ln^2\varepsilon_m}{\ln\varepsilon_t}\right]. \tag{54}$$

The differences between the approximate solution (50) with Eqs. (43) and (51) and the corresponding simplified solution (50) with Eqs. (43) and (54) are so small that for most curves they are invisible in Fig. 8. Therefore,
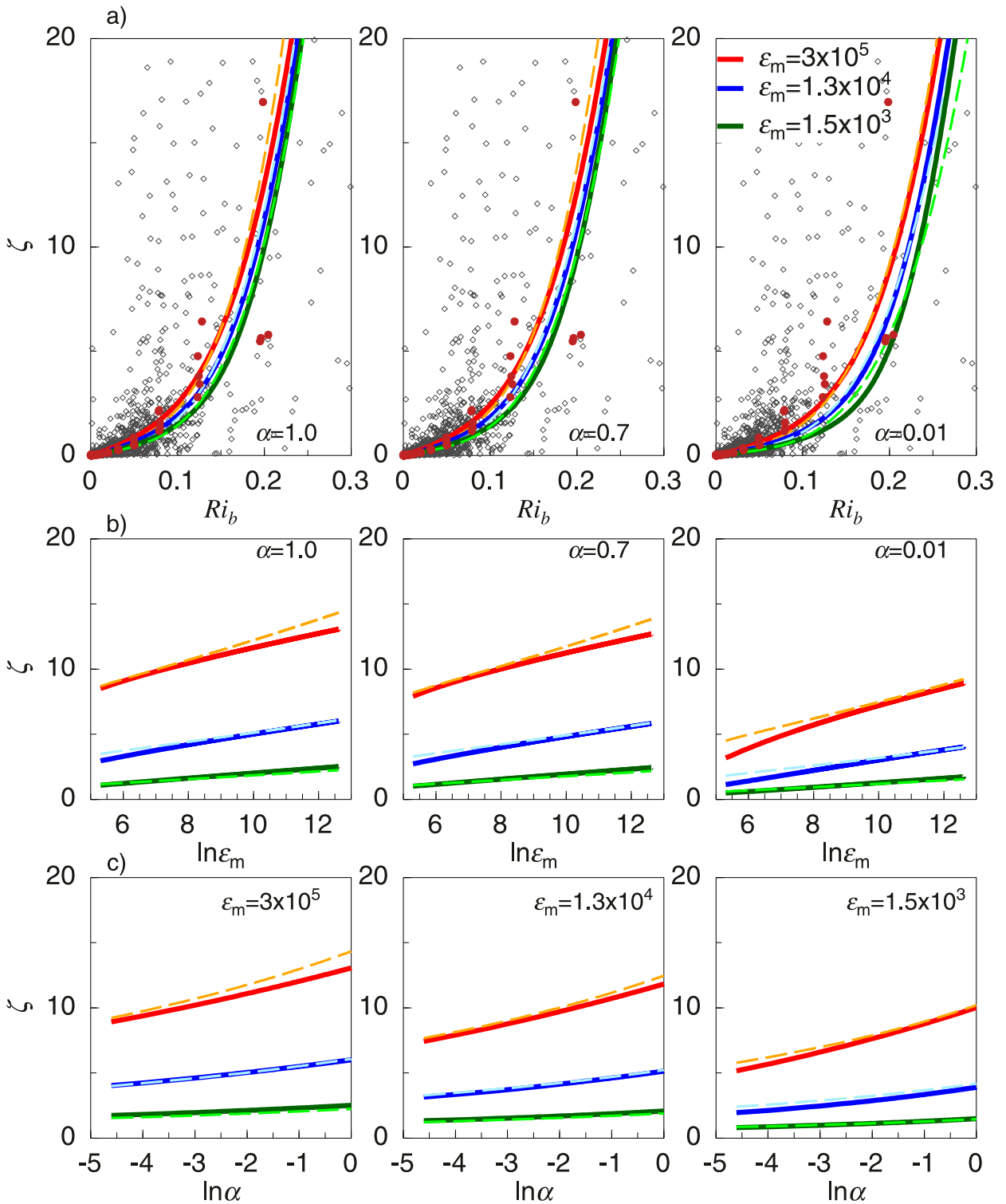
FIG. 8. The stability parameter $\zeta = z/L$ as a function of (a) Ri_b, (b) ε_m, and (c) α. The solid lines show the exact solutions of the governing MOST Eq. (23) obtained with the GLGS functions (34) and (35). The dashed lines represent results of the new parameterization [Eqs. (50)–(53) and with Eq. (43)]. The same curves describe also the simplified parameterizations [Eqs. (50) with Eqs. (43) and (54)], since the difference between results of both parameterizations are invisible in the figures. In (b) and (c) curves are shown for Ri_b equal to 0.1 (green), 0.15 (blue), and 0.2 (red). Gray and brown symbols represent SHEBA measurements as in Fig. 4.

in the following we will use only the simplified equation without loss of accuracy.

Finally, it is worth stressing a drawback of our semi-analytical solution. It does not result in the exact asymptotic behavior of transfer coefficients for $Ri_b \to \infty$. But this is not a serious problem because the numerical values of exponents γ for the exact and approximate solutions are very close to each other. The small difference appears due to our intention to achieve a high accuracy in the finite range $0 < Ri_b < 0.2$.

9. Parameterization of transfer coefficients and guide for implementation in climate models

When the approximate solution for the stability parameter $\zeta(\widehat{Ri}_b, \varepsilon_m, \varepsilon_t)$ is known, the explicit formulas for the normalized transfer coefficients are obtained algebraically by inserting Eq. (50) into Eq. (34) for the stability function $\psi_m(\zeta)$ and in Eq. (35) for the function $\psi_h(\zeta)$. Then the result is used in Eqs. (19) and (20), where the small terms $\psi_m(\zeta_a/\varepsilon_m)$ and $\psi_h(\zeta_a/\varepsilon_m)$ can be neglected without loss of accuracy as described above. Thus, we obtain

$$f_m = \left(1 + \frac{50.0}{\ln \varepsilon_m}\left\{\left[1 + 0.3\left(\frac{\ln^2 \varepsilon_m}{\ln \varepsilon_t}\widehat{Ri}_b \right.\right.\right.\right.$$
$$\left.\left.\left.\left. + A\widehat{Ri}_b^{3.625})\right]^{1/3} - 1\right\}\right)^{-2} \quad (55)$$

and similarly

$$f_h = f_m^{1/2}\left\{1 + \frac{12.5}{\ln \varepsilon_t}\ln\left[1 + 0.40\left(\frac{\ln^2 \varepsilon_m}{\ln \varepsilon_t}\widehat{Ri}_b + A\widehat{Ri}_b^{3.625}\right)\right]\right\}^{-1}, \quad (56)$$

with the coefficient A given by Eq. (54).

The curves showing these functions are presented in Fig. 9 for the exact solution and for its approximated counterpart. For comparison, in the same figures (here and in following) the lowermost solid lines visualize the transfer coefficients based on the integrated Businger–Dyer stability functions (14).

Finally, using Eqs. (55) and (56) in Eqs. (17), we find the formulas for the transfer coefficients C_d and C_h as

$$C_d = \frac{\kappa^2}{\left(\ln \varepsilon_m + 50.0\left\{\left[1 + 0.3\left(\frac{\ln^2 \varepsilon_m}{\ln \varepsilon_t}\widehat{Ri}_b + A\widehat{Ri}_b^{3.625}\right)\right]^{1/3} - 1\right\}\right)^2}, \quad (57)$$

$$C_h = \frac{\kappa C_d^{1/2}}{\ln \varepsilon_t + 12.5\ln\left[1 + 0.40\left(\frac{\ln^2 \varepsilon_m}{\ln \varepsilon_t}\widehat{Ri} + A\widehat{Ri}_b^{3.625}\right)\right]}, \quad (58)$$

with the function $A(\varepsilon_m, \varepsilon_t)$ given by Eq. (54) in both transfer coefficients.

In Fig. 10 we show the transfer coefficients C_d and C_h as a function of $\widehat{Ri}_b$ for given ε_m and α. As expected, the transfer coefficients are equal to the neutral limit at $\widehat{Ri}_b = 0$ for all ε_m and ε_t, and they decrease monotonically when $\widehat{Ri}_b$ increases. This dependence is very common for all transfer coefficients and is in agreement with measurements. The difference between the exact and approximate C_d and C_h is smaller than 5% in the range $0 \le \widehat{Ri}_b \le 0.2$, which is most often observed (see G2007a; Grachev et al. 2013).

The agreement is that high because the approximate solutions (57) and (58) reproduce the exact ones in the limit $\widehat{Ri}_b \to 0$ for all values of a_m, b_m, a_h,

and b_h. And, moreover, in the opposite limit $\zeta \to \infty$ the asymptotes

$$f_m \sim \frac{1}{\zeta^{2/3}} \sim \frac{1}{\widehat{Ri}_b^{2.42}}, \quad f_h \sim \frac{1}{\zeta^{1/3}\ln\zeta} \sim \frac{1}{\widehat{Ri}_b^{1.21}\ln\widehat{Ri}_b} \quad (59)$$

also approach the exact solution

$$f_m \sim \frac{1}{\zeta^{2/3}} \sim \frac{1}{\widehat{Ri}_b^2}, \quad f_h \sim \frac{1}{\zeta^{1/3}\ln\zeta} \sim \frac{1}{\widehat{Ri}_b\ln\widehat{Ri}_b}. \quad (60)$$

The asymptotes (59) for $Ri_b \to \infty$ easily follow from Eqs. (57) and (58) using asymptotic expansion in the small parameter $1/Ri_b$.

Thus, the Eqs. (57) and (58) with Eq. (54) represent the main result of this work. Due to the compact functional form of the GLGS functions they provide new, explicit noniterative parameterizations of the transfer coefficients C_d and C_h as a function of $\widehat{Ri}_b$ for given parameters Pr_0, ε_m and ε_t. When the parameterizations are implemented in a model we recommend testing a hierarchy, by using either
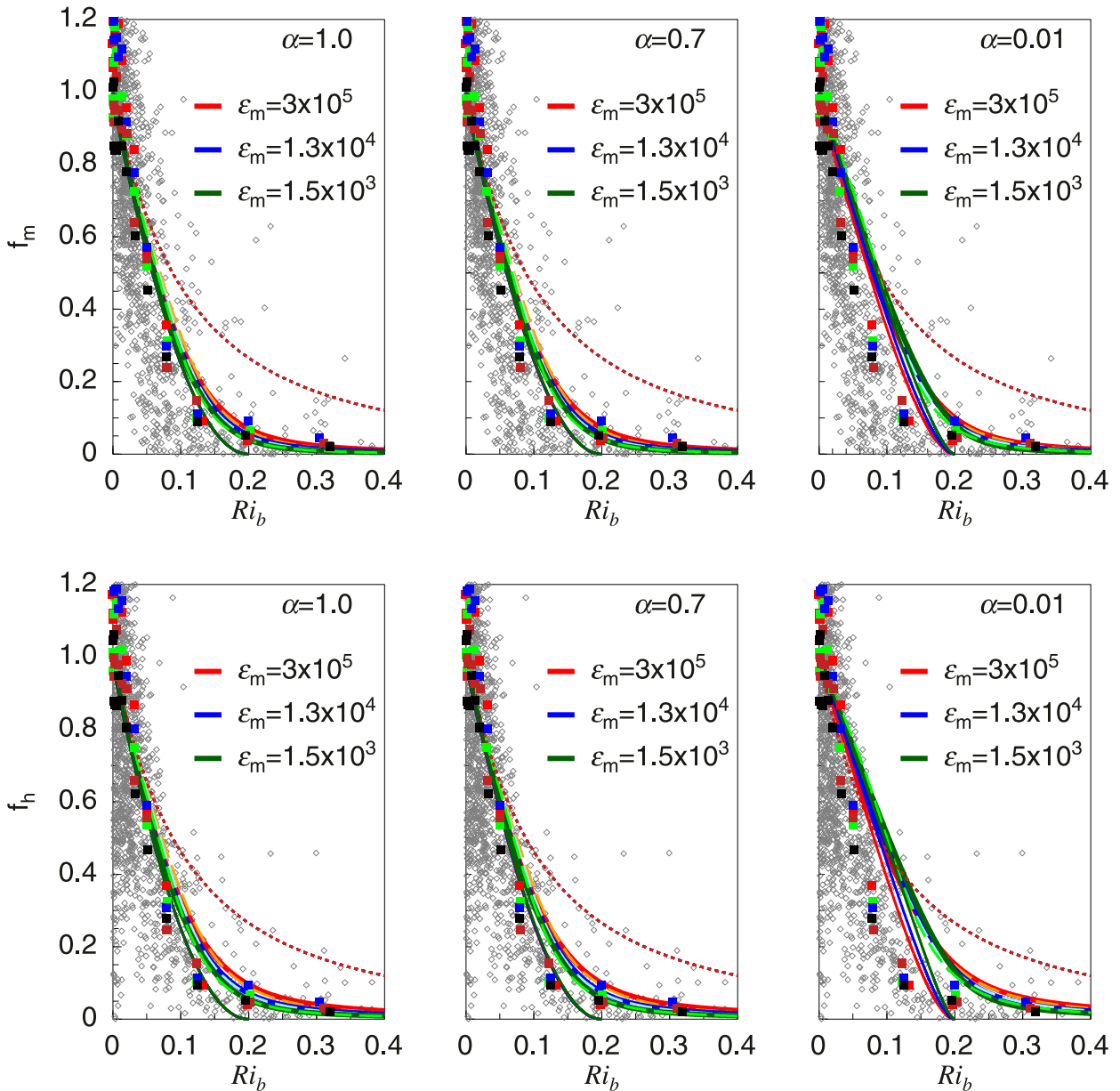
FIG. 9. Normalized transfer coefficients f_m and f_h as a function of Ri_b for given ε_m and α. The thick solid lines show the coefficients obtained using the exact solutions of the governing MOST Eq. (23) based on the GLGS functions (34) and (35). Thin solid lines with $f_m = f_h = 0$ for $Ri_b \geq$ 0.2 represent the solution based on the Businger–Dyer stability functions. The dashed green, red, and blue lines show the parameterizations (55) and (56). Brown dashed lines refer to the parameterization by Louis (1979) [Eq. (65)]. The gray symbols are the SHEBA data at all levels averaged over 1 h. Colored squares represent bin averages of measurements at different heights where the color coding is as in Fig. 5.

representative values for both ε_m and ε_t (level 1) or a representative value for ε_m and assume $\varepsilon_m = \varepsilon_t$ (level 2). Using these assumptions, simplified analytical expressions for C_d and C_h can be easily derived.

10. Comparison with earlier parameterizations

In this section we compare the noniterative parameterizations of transfer coefficients based on the GLGS

functions with earlier noniterative parameterizations of Gryanik and Lüpkes (2018), which are based on the G2007a stability functions, and with parameterizations of Louis (1979) and Louis et al. (1981), which are often used in climate models.

Parameterizations of the transfer coefficients C_d and C_h based on the G2007a stability functions were given already by Gryanik and Lüpkes (2018). Their explicit formulae, expressing C_d and C_h in terms
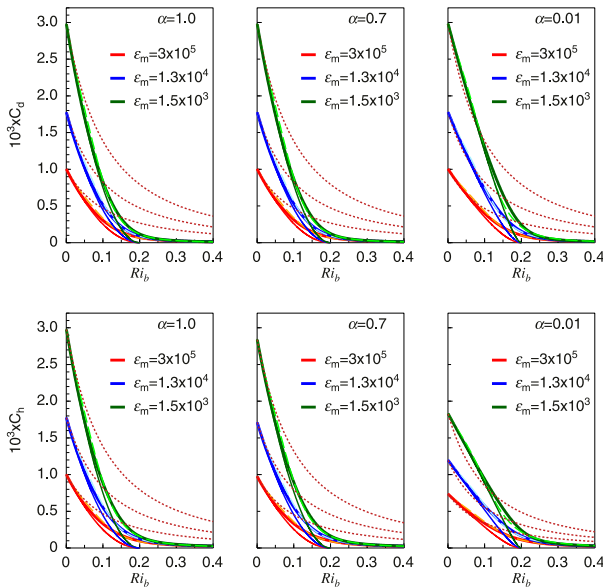
FIG. 10. Transfer coefficients (top) C_d and (bottom) C_h at 10 m height as a function of Ri_b. The thick solid lines show the coefficients obtained using the exact (iterative) solutions of the governing MOST Eq. (23) based on the GLGS functions (34) and (35) for ε_m and α as indicated in the figure. Dashed green, blue, and red lines represent the results of the approximations (57) and (58). Brown dashed lines refer to the parameterization by Louis (1979) [Eq. (65)]. Measurements are shown in Figs. 5 and 6.

of the bulk Richardson number Ri_b, ε_m, and ε_t are given by Eqs. (17) with the neutral values of C_{dn} and C_{hn} from Eq. (18) and with the functions f_m and f_h given by

$$f_m = \left\{ 1 - \frac{1}{\ln\varepsilon_m}\left[10.29 - 19.5x + 2.18\ln\frac{(x+0.67)^2}{x^2-0.67x+0.45} \right.\right.$$

$$\left.\left. + 7.54\arctan(1.725x - 0.58) \right]\right\}^{-2}, \qquad (61)$$

$$f_h = f_m^{1/2}\left\{ 1 - \frac{1}{\ln\varepsilon_t}\left[2.16 - 2.5\ln(1 + 3\zeta + \zeta^2) \right.\right.$$

$$\left.\left. + 1.12\ln\frac{\zeta+0.38}{\zeta+2.62} \right]\right\}^{-1}, \qquad (62)$$

where $x = (1+\zeta)^{1/3}$ and ζ is provided by the parameterization of the stability parameter

$$\zeta = \frac{\ln^2\varepsilon_m}{\ln\varepsilon_t}Ri_b + \frac{(\ln\varepsilon_m + 11.3)^{3.82}}{11.5(\ln\varepsilon_t + 6.4)^{1.91}}\left[\frac{(\ln\varepsilon_m + 11.3)^2}{\ln\varepsilon_t + 6.4}\right.$$

$$\left. - \frac{\ln^2\varepsilon_m}{\ln\varepsilon_t}\right]Ri_b^{2.91}. \qquad (63)$$

These parameterizations were derived for the same ranges of stability Ri_b and roughness parameters ε_m and ε_t as considered in the present work. The optimal values for the exponent γ and the parameter ζ_a related to the G2007a stability functions were determined as

$$\gamma = 2.92, \quad \zeta_a = 3.6. \qquad (64)$$

Thus, especially the value for ζ_a differs from the value 7.25 related to the GLGS functions.

Figure 11 shows the differences between the functions f_m and f_h following from Eqs. (61) and (62) and from Eqs. (55) and (56). Obviously, the scheme based on the G2007a functions produces too large values of f_m and f_h in the region $Ri_b > 0.1$ although there is a large improvement relative to the Louis (1979), Louis et al. (1981), and Launiainen (1995) schemes as discussed in Gryanik and Lüpkes (2018). We refer the reader to the latter work for a detailed study of differences between their scheme and earlier ones. We just stress here that relative to the SHEBA data a significant overestimation of momentum and heat fluxes by Louis (1979) was found and that the essential dependence of f_m and f_h functions on roughnesses and their interplay with stability effects was completely absent. But as Fig. 12 shows, due to the overestimation of f_m and f_h in the very stable range, also C_d and C_h are overestimated when the original G2007a functions are chosen. This would lead to an overestimation of the fluxes as well.

Concerning the dependence on roughness we add here one important point, which was not yet mentioned by Gryanik and Lüpkes (2018). Many models use approaches as those of Louis (1979) and Louis et al. (1981) where the normalized transfer coefficients depend on Ri_b only. For example, the parameterization, which is used in the ECMWF model for a long time, applies the simple parameterization

$$f_m = \frac{1}{(1 + bRi_b)^2}, \qquad (65)$$

with the numerical constant $b = 4.7$. When this parameterization is used in Eq. (17), C_d and C_h depend on the roughness parameter ε_m only due to the corresponding dependence of C_{dn} and C_{hn}. Louis derived the functional form and adjusted the coefficients of his parameterization (65) on the basis of the Businger–Dyer stability functions, due to which the fluxes of momentum and heat amount to zero for a Richardson number larger than the critical one. At the time of the derivation of the Louis approach these were the only well documented stability functions. Using the Businger–Dyer stability correction functions Louis
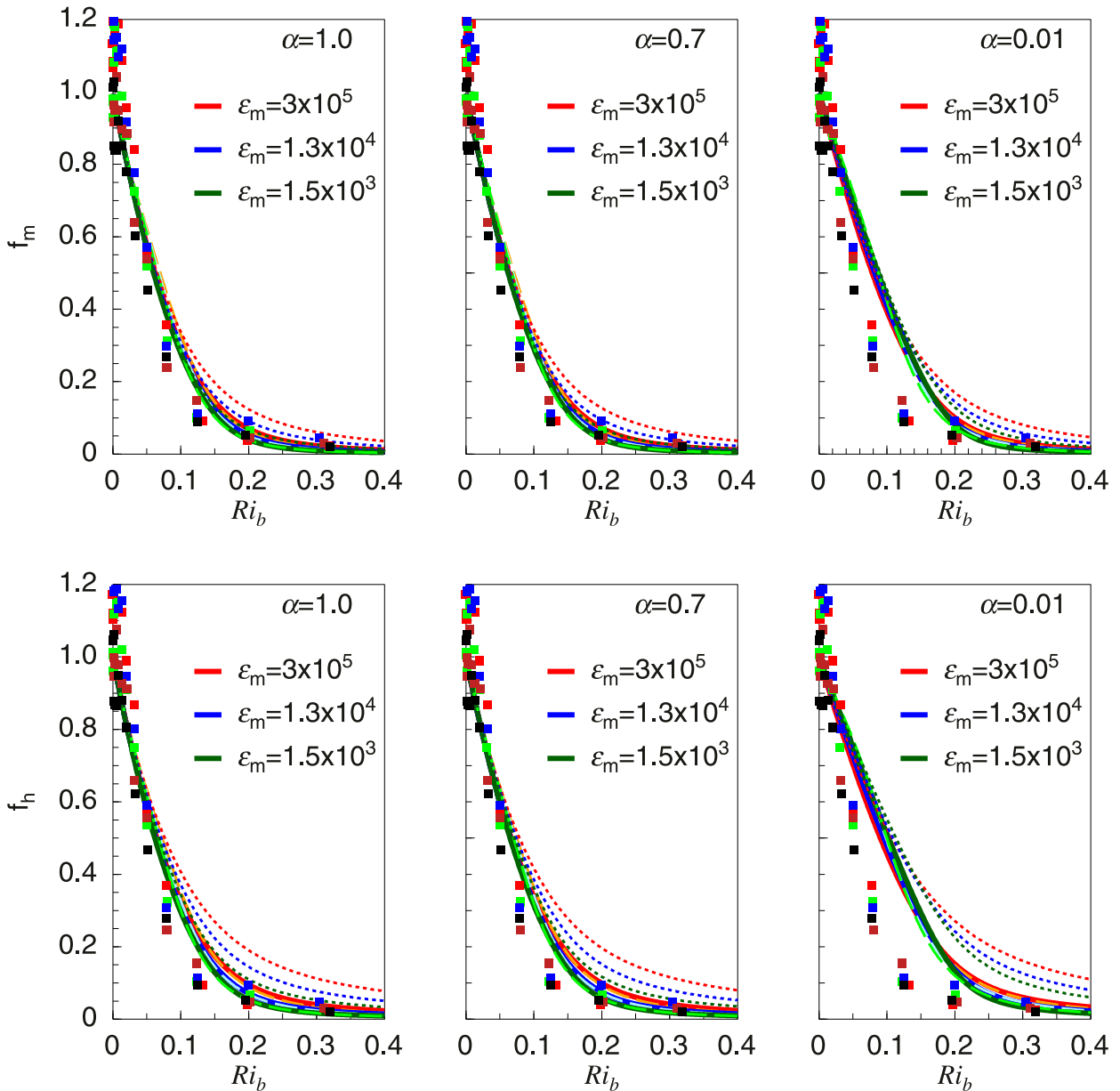
FIG. 11. As in Fig. 9, but short-dashed lines refer to results obtained with the original stability functions of G2007a.

computed f_m and f_h as functions of Ri_b for different $\varepsilon_m = \varepsilon_t$ and then proposed the best fit for all curves. Implicitly such a fit assumes the existence of some representative ε_m for a relevant range of roughness. For the Businger–Dyer stability functions the dependence of the normalized transfer coefficients on the roughness, is indeed, very small (see, e.g., Fig. 2 in Gryanik and Lüpkes 2018). So, they were approximated by Louis as depending only on stability. Later, the Louis approach was applied without discussion to many other stability functions. Delage (1997) adjusted the only coefficient b of the parameterization (65) to the new value $b = 12$. This value was

optimal to fit results based on the stability functions of Beljaars and Holtslag (1991), which do not contain a critical Richardson number.

All this shows that there are important conceptual differences between the parameterizations of Louis and the new ones.

11. Discussion

In this section we discuss the flexibility and robustness of the GLGS functions. Finally, we provide an overview of the assumptions and important constraints.
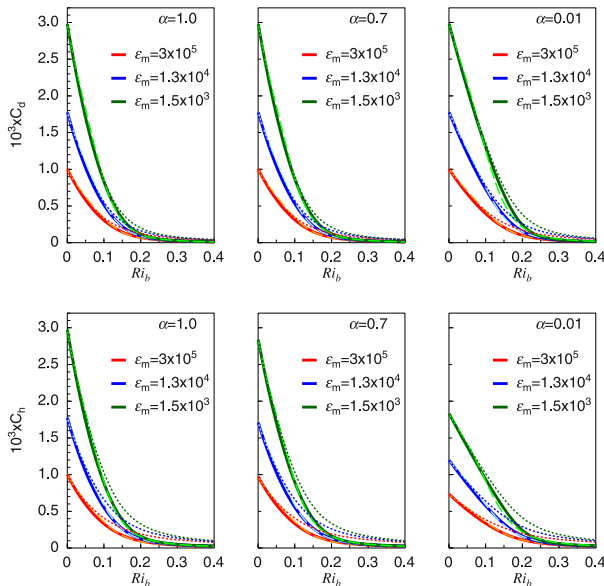
FIG. 12. As in Fig. 10, but short-dashed lines refer to results obtained with the original stability functions of G2007a.

a. The flexibility/robustness of the new stability functions

Our analysis of the previous sections revealed that the functional form of the GLGS functions is flexible in the sense that they can be used for an optimal approximation not only of the nondimensional gradients, but also of the stability parameter–bulk Richardson number relationship. It was demonstrated that the assumptions for the optimization offer constraints for the empirical constants. However, the following questions can be asked: How robust are the values of these constants and how far does the accuracy of the nondimensional gradients decrease when only the $\zeta(\mathrm{Ri}_b)$ dependence is optimized?

To answer these questions we performed a sensitivity analysis, which is presented in detail in appendix D. Summarizing the results, our analysis shows that it is extremely difficult to establish an accurate approximation of the stability functions fulfilling all requirements, namely, to minimize the differences to the observed flux–gradient and flux–profile relationships and to the transfer coefficients using the same empirical constants a_m, b_m, a_h, b_h, and Pr_0. The optimal set of parameters for one of the relationships differs significantly from the optimal set for the other relationship. However, we stress that the GLGS functions provide a reasonable compromise solution when the set of parameters (38) is used.

Furthermore, it is possible to define a set of constants, for which the $\zeta(\mathrm{Ri}_b)$ relationship and the transfer coefficients can almost not be distinguished from those based

on the original G2007a functions. This result is important because it shows that the G2007a functions could be replaced by a simpler formulation just for practical reasons, namely, to save computing time in climate and weather prediction models.

Finally, we stress that important constraints, which were imposed on the original stability functions of G2007a (their constraints i–iii, p. 328) are approximately satisfied by the GLGS functions (34) and (35) as well. So, the limit of the modified ϕ_m function for $\zeta \to \infty$ is $(a_m/b_m^{2/3})\zeta^{1/3}$. With the proposed values $a_m = 5$ and $b_m = 0.3$ we obtain the numerical limit $11.2\zeta^{1/3}$ compared to $6.5\zeta^{1/3}$ as obtained from the corresponding G2007a function. We argued that this difference causes only a small discrepancy in the near-neutral range due to the relatively small sensitivity of the ϕ_m function to b_m. However, it became important for a better reproduction of the SHEBA data for stronger stability. The limit of the modified ϕ_h function for $\zeta \to \infty$ is a constant equal to $1 + a_h/b_h = 12.5$ (using $\mathrm{Pr}_0 = 1.0$). This is twice larger than the value 6.0 of G2007a and than the value 6.2 resulting from functions by Webb (1970). For the SHEBA data the limit is reached already for $\mathrm{Ri}_b > 10$. One can see also that the larger limit 12.5 is still in the scatter of the SHEBA data. The value $a_h = 5.2$ by Webb (1970) is similar to the value 6.0 found by G2007a and very close to our result $a_h = 5.0$, if one accepts the accuracy estimation of 30% by Webb (1970) and Högström (1996) for the MOST coefficients. Although until today the physical mechanisms explaining the scatter of a_h for large stability are unknown, the levelling of ϕ_h is well documented by measurements. It is attributed to the nonstationarity of turbulence at the large stability limit (Mahrt 2007) and to the ceasing of developed Kolmogorov turbulence in the range of large stability (Grachev et al. 2013).

b. Overview of assumptions and important constraints

Our assumptions are the following ones:

(i) The universal functions depend linearly on ζ at small ζ, namely, $\phi_m \approx 1 + a_m\zeta$ and $\phi_h(\zeta) \approx 1 + a_h\zeta$ for $\zeta \to 0$. The universal function for momentum ϕ_m is proportional to $\zeta^{1/3}$ in the limit $\zeta \to \infty$, but the function for heat ϕ_h approaches a constant value $\mathrm{Pr}_0(1 + a_h)$ in the same limit $\zeta \to \infty$.

(ii) The stability functions fit the measured data in the available range of the stability parameter ζ, simultaneously approximating the flux–nondimensional gradient relationship and the stability parameter–bulk Richardson number (ζ–Ri_b) relationship reasonably well.

(iii) Both functions $\phi_m(\zeta)$ and $\phi_h(\zeta)$ are analytically integrable functions of ζ resulting in analytically tractable stability correction functions $\psi_m(\zeta)$ and $\psi_h(\zeta)$.

(iv) The functions $\psi_m(\zeta)$ and $\psi_h(\zeta)$ and their derivatives do not have any singularities at $\zeta = 0$, thus allowing a continuous matching with the stability functions in the unstable range $\zeta < 0$.

(v) The stability correction functions $\psi_m(\zeta)$ and $\psi_h(\zeta)$ are applicable for all ζ, i.e., provide reasonable physical characteristics of the bulk transfer coefficients. They must be monotonically decreasing functions with respect to the stability parameter ζ (Sharan and Kumar 2010).

The assumption (i) on the limit $\zeta \to 0$ is probably the most solid one. The asymptotic limit $\zeta \to 0$ (often called log-linear limit, or limit of the Businger–Dyer stability function, or simply Businger–Dyer limit) is well supported by data from field measurements, laboratory experiments and numerical simulations. It holds for a limited range of stability $0 < \zeta < 0.08$ (corresponding to $0 < \mathrm{Ri}_b < 0.05$ for the stability functions of G2007a). This fact is well documented by earlier studies (see, e.g., Businger et al. 1971; Webb 1970), as well as by results of recent field measurements (see, e.g., G2007a). However, the region of validity of the log-linear asymptotes depends on the used stability functions (see Fig. 1).

The constraint (i) on the limit $\zeta \to \infty$ is less solid. As shown by G2007a, the asymptote for ϕ_m (often called u^*-less limit) holds for very large ζ. But in this range the measurement of fluxes is difficult due to their small values. The asymptote for $\phi_h(\zeta)$, which levels off at large ζ, is also very uncertain in the range of extremely large stability. The reason is again related to the difficulty of measuring small heat fluxes. Both the stability functions for momentum and for heat have an accuracy not higher than 20%–30% (see, e.g., Webb 1970; Foken 2006). The plots in Fig. 1b also demonstrate that the asymptotes (ii) are not accepted by all authors.

The constraint (ii) is satisfied by the GLGS functions by construction.

The constraint (iii) guaranties a reasonably simple analytically tractable functional form of stability correction functions $\psi_m(\zeta)$ and $\psi_h(\zeta)$. From a first point of view the constraint (iii) has a technical character and has no obvious theoretical support. However, keeping in mind that wind speed and temperature profiles are explicitly involved in the calculation of many physical characteristics of the stable surface layer, the constraint (iii) becomes practically very desirable. Corresponding benefits were already discussed in section 7 in details.

The constraint (iv) of a smooth matching with the convective stability range ($\zeta < 0$) is realized for the

GLGS functions without problems. Indeed, the argument of analyticity at $\zeta = 0$ holds due to the linear dependence of $\psi_m(\zeta)$ and $\psi_h(\zeta)$ on ζ for $\zeta \to 0$. This constraint actually is not new. Louis (1979) applied this constraint to establish continuous and smooth transfer coefficients at $\mathrm{Ri}_b = 0$ in numerical models. From Eqs. (34) and (35) it is obvious that continuity and smoothness of transfer coefficients in Ri_b immediately follows from continuity and smoothness of the $\psi_m(\zeta)$ and $\psi_h(\zeta)$ functions in ζ [see Eqs. (34) and (35)] and vice versa.

The constraint (v) suggested by Sharan and Kumar (2010) implies that

$$\frac{dC_k}{d\zeta} \le 0, \quad C_k(0) = C_{kn}, \quad k = [d, h] \qquad (66)$$

for any given stability correction function $\psi_m(\zeta)$ and $\psi_h(\zeta)$ in the range $0 \le \zeta \le \infty$ and for all relevant values of the roughness parameters. This hypothesis is based on, and supported by, all measurements that are known nowadays with reasonable accuracy. The constraint (66) provides a rigorous criterion for the upper bound of the region of applicability of the stability correction functions ψ_m and ψ_h. Sharan and Kumar (2010) used the criterion in order to prove that the stability functions of G2007a are applicable for all ζ. It is expected that the GLGS functions (34) and (35) are applicable as well, since they closely approximate the functions of G2007a. Our straightforward analysis (see appendix C) indeed leads to the conclusion that the inequalities (66) are satisfied by the GLGS functions. If so, the GLGS functions are applicable and have no upper bound for the region of applicability, similar to the G2007a functions.

Finally, to the best of our knowledge, the above full list of constraints was never formulated before explicitly. The establishing of constraints is important not only for empirical stability functions. They can be interpreted also in a more general context, i.e., as constraints, which must be imposed on any stability function, derived theoretically from advanced closure models of second and higher order. Even when the equations for stability functions can be derived from the set of second-order or third-order closure model equations, the solution of these equations provides stability functions in implicit form (see, e.g., Canuto et al. 1994). Their inversion, as a rule, cannot be carried out analytically, so only a numerical or an approximate analytical method of inversion can be used. In the latter case the described constraints provide a guiding line, to avoid erroneous results. The same is true also for spectral closure models (e.g., Sukoriansky et al. 2005; Galperin and Sukoriansky 2010). Their complex results obtained by rigorous theoretical methods require a fractional polynomial fit to obtain a

simple functional form of stability functions in the context of MOST (see Sukoriansky 2008; Tastula et al. 2015). For fitting the knowledge of constraints is very useful.

Summarizing, we have shown that all constraints (i) to (v) are fulfilled by the GLGS functions (33) and (33) so that they are established correctly.

12. Summary and conclusions

This work starts with a summary of prior investigations by G2007a, of Grachev et al. (2015) and Gryanik and Lüpkes (2018) concentrating on the use of SHEBA data for the parameterization of near-surface fluxes of heat and momentum. Based on these publications a modification and extension of the G2007a and Grachev et al. (2015) formulation of the MOST stability functions is proposed. This results in corresponding parameterizations of transfer coefficients for momentum and heat. The most important results can be summarized as follows:

1) The newly derived stability functions (GLGS) have the same accuracy with respect to data as the original stability functions by G2007a, but their functional form is simpler, so that they are well suited for a practical application in weather and climate models.
2) The new functions are extended to account for their dependence on the neutral-limit turbulent Prandtl number Pr_0, the effect of which was not included in the original formulation. As was shown later by Sorbjan and Grachev (2010) Pr_0 can have a significant impact on momentum and heat transfer.
3) For the adjustment of the new functions to measurements we followed a new strategy. Namely, free constants were chosen to represent both the observed flux–nondimensional gradient relationship, the ζ–Ri_b relationship and the stability dependence of transfer coefficients for heat and momentum simultaneously.
4) It is shown that the GLGS functions are slightly superior to the G2007a functions with respect to the representation of the stability parameter–bulk Richardson number relationship, so also to the corresponding transfer coefficients for momentum and heat.
5) The applicability of the modified and extended GLGS stability functions is proven for all values of the stability parameter ζ using a method proposed by Sharan and Kumar (2010).
6) Using the GLGS functions new noniterative bulk parameterizations of the transfer coefficients of momentum and heat are obtained following an approach of Gryanik and Lüpkes (2018). The transfer coefficients are formulated as functions of the bulk Richardson

number Ri_b, of the neutral-limit turbulent Prandtl number Pr_0 and of the nondimensional roughness parameters for momentum $\varepsilon_m = z/z_0$ and heat $\varepsilon_t = z/z_t$.
7) By comparison with SHEBA data it is shown that traditional parameterizations underestimate or overestimate the transfer coefficients for large Ri_b depending on the prescribed value of Pr_0. The new transfer coefficients agree better with SHEBA data for strong stability ($Ri_b > 0.1$) than previous parameterizations and they agree well with those based on the Businger–Dyer functions in the range $Ri_b \leq 0.1$.
8) It is shown that roughness has a significant effect on the stability dependence of the transfer coefficients when the new stability functions are used. This confirms a result of Gryanik and Lüpkes (2018) based on the G2007a functions.
9) Finally, for the practical application in weather and climate models we proposed a hierarchy of the new noniterative parameterizations of different levels of complexity.

Summarizing, we state that the new noniterative surface-layer scheme is superior to other schemes describing the turbulent mixing in polar regions and probably everywhere on Earth, so that we recommend it for practical use. We think that biases in the results of climate models during stable stratification should not be avoided by enhancing the efficiency of turbulent mixing. Other mechanisms, e.g., of ice/snow–atmosphere interaction can be responsible for such biases.

We recommend modelers to test the new scheme in weather prediction and climate models, where it can be easily implemented. Although, the new parameterizations are proposed for the calculation of turbulent surface-layer fluxes over sea ice covered polar regions during neutral and stable stratification (for a range of parameters that is comparable with SHEBA data), in principle, they can be used everywhere in models where MOST stability functions can be applied [see discussion by Gryanik and Lüpkes (2018) and by Srivastava et al. (2020)].

APPENDIX A

List of Stability Functions ϕ_k and Stability Correction Functions ψ_k

Below, we list the most often used stability functions and stability correction functions in addition to those of Businger–Dyer and G2007a. These are the functions of Holtslag and De Bruin (1988), Beljaars and Holtslag (1991), Chenge and Brutsaert (2005), and Sukoriansky (2008), which we write in their traditional forms and mention also their region of applicability. We remind the reader that the stability functions of Businger–Dyer have originally been adjusted to the range $0 < \zeta < 1$.

The stability functions of Holtslag and De Bruin (1988) assume the Rayleigh analogy between momentum and heat, which means that $\phi_m(\zeta) = \phi_h(\zeta)$. The functions are given as

$$\phi_m(\zeta) = \phi_h(\zeta) = 1 + a\zeta + b\zeta(1 + c - d\zeta)\exp(-d\zeta),$$
$$0 \le \zeta < 10. \quad \text{(A1)}$$

The corresponding stability correction functions read as

$$\psi_m(\zeta) = \psi_h(\zeta) = -a\zeta - b\left(\zeta - \frac{c}{d}\right)\exp(-d\zeta) - \frac{bc}{d},$$
$$0 \le \zeta < 10, \quad \text{(A2)}$$

with the four constants $a = 0.7$, $b = 0.75$, $c = 5$, and $d = 0.35$ for both $\psi_m(\zeta)$ and $\psi_h(\zeta)$.

Beljaars and Holtslag (1991) proposed for momentum the stability function (A2) of Holtslag and De Bruin (1988), but the new function for heat is given as

$$\phi_h(\zeta) = 1 + a\zeta\left(1 + \frac{2a}{3}\zeta\right) + b\zeta(1 + c - d\zeta)\exp(-d\zeta),$$
$$0 \le \zeta < 10, \quad \text{(A3)}$$

$$\psi_h(\zeta) = -\left(1 + \frac{2a}{3}\zeta\right)^{3/2} + 1 - b\left(\zeta - \frac{c}{d}\right)\exp(-d\zeta) - \frac{bc}{d},$$
$$0 \le \zeta < 10, \quad \text{(A4)}$$

with the same four constants $a = 1$, $b = 0.667$, $c = 5$, and $d = 0.35$ for both $\psi_m(\zeta)$ and $\psi_h(\zeta)$.

The functions of Chenge and Brutsaert (2005) are defined as

$$\phi_k(\zeta) = 1 + a_k \frac{\zeta + \zeta^{b_k}(1 + \zeta^{b_k})^{(1-b_k)/b_k}}{1 + (1 + \zeta^{b_k})^{1/b_k}}, \quad 0 \le \zeta < 5 \quad \text{(A5)}$$

and

$$\psi_k(\zeta) = -a_k \ln[\zeta + (1 + \zeta^{b_k})^{1/b_k}], \quad 0 \le \zeta < 5, \quad \text{(A6)}$$

where $k = [m, h]$. Here $a_m = 6.1$ and $b_m = 2.5$ for the momentum stability function ($k = m$) and $a_h = 5.3$ and $b_h = 1.1$ for the heat stability function ($k = h$).

Sukoriansky (2008) established the stability functions

$$\phi_m = 1 + 2.25\zeta - 0.4\zeta^2, \quad 0 \le \zeta < 2.81 \quad \text{(A7)}$$

and

$$\phi_h = 0.7[1 + 2\zeta - 0.7\zeta(\zeta - 1/2)^4], \quad 0 \le \zeta < 1.64. \quad \text{(A8)}$$

The corresponding stability correction functions ψ_m and ψ_h are

$$\psi_m = -(2.25\zeta - 0.2\zeta^2), \quad 0 \le \zeta < 2.81 \quad \text{(A9)}$$

and

$$\psi_h = -0.7\{2\zeta + 0.14[(\zeta - 1/2)^5 + (1/2)^5]\},$$
$$0 \le \zeta < 1.64. \quad \text{(A10)}$$

Here, a misprepresentation of functions (A9) and (A10) by Sukoriansky (2008) is corrected. All corrections have been accepted by S. Sukoriansky (2017, private communication).

In contrast to empirically based functions the functions of Sukoriansky (2008) do not have free parameters. All coefficients given in Eqs. (A7) and (A8) have been derived rigorously under several well established assumptions (see Sukoriansky and Galperin 2013, and references therein).

APPENDIX B

Dependence of Stability Functions on Pr_0

In this appendix we clarify some issues related with the definition of the stability function ϕ_h and stability correction function ψ_h and their dependences on the neutral-limit turbulent Prandtl number Pr_0.

The Prandtl number Pr in general and its neutral limit in particular represent important characteristics of turbulent flows. It is a measure of the relative importance

of mechanical and thermal mixing. Physically, the assumption $\text{Pr} \neq 1$ originates from the conceptual differences between length and time scales of dissipation/mixing for momentum and heat.

Although observable physical characteristics of the surface layer are invariant with respect to any definition of the dependence on Pr_0, the functional forms of the MOST equations and stability functions depend on this definition. Establishing an empirical value of Pr_0 depends not only on an agreement on the functional form of the stability functions ϕ_m and ϕ_h in the limit of vanishing stratification, but—as becomes clear, e.g., from Eq. (B1) below—also on the used value of the von Kármán constant and on the definition of the Obukhov length L. Several researchers prefer not to use Pr_0 at all and use the von Kármán constant for temperature κ_t instead (see, e.g., Zilitinkevich et al. 2002; Zilitinkevich and Esau 2007). Then the constant κ_t is introduced similar to the von Kármán constant κ as a matter of convenience to ensure $\phi_h(0) = 1$. In this case Pr_0 is defined as $\text{Pr}_0 = \kappa/\kappa_t$. Zilitinkevich et al. (2002) used, e.g., $\kappa = 0.4$ and $\kappa_t = 0.42$ so that $\text{Pr}_0 = 0.95$.

In the main text of our work we use the definition (1) for the Obukhov length following Monin and Yaglom (1971) with $\kappa = 0.4$ as in Högström (1988) and with the multiplicative formulation of ϕ_h where Pr_0 occurs as a factor. The normalization conditions are given by Eqs. (6) and (7). This follows the traditional line accepted by the modeling community.

Another possibility, which is often used for the processing of measurements (Andreas 1987; Foken 2017) is to use Eq. (4) for momentum with the normalization (6) together with

$$\frac{\kappa z}{\text{Pr}_0 \theta_*} \frac{d\Theta}{dz} = \phi_h(\zeta), \qquad (B1)$$

with the normalization

$$\phi_h(0) = 1. \qquad (B2)$$

In this case, for self-consistency, Eqs. (11) must be replaced by

$$\psi_k(\zeta) = \int_0^\zeta \frac{1 - \phi_k(\zeta')}{\zeta'} d\zeta', \quad \phi_k(\zeta) = 1 - \zeta \frac{d\psi_k}{d\zeta}, \quad k = [m, h]. \qquad (B3)$$

The governing MOST equation reads then

$$\widehat{\text{Ri}}_b = \frac{(1 - 1/\varepsilon_m)^2}{1 - 1/\varepsilon_t} \zeta \frac{\ln\varepsilon_t - [\psi_h(\zeta) + \psi_h(\zeta/\varepsilon_t)]}{[\ln\varepsilon_m - \psi_m(\zeta) + \psi_m(\zeta/\varepsilon_m)]^2},$$

$$\widehat{\text{Ri}}_b = \frac{\text{Ri}_b}{\text{Pr}_0}. \qquad (B4)$$

If an alternative definition is preferred it is straightforward to reformulate our results in terms of this definition. For example, Businger et al. (1971) formulated the log-linear stability function for heat as $\phi_h(\zeta) = 0.95 + 7.8\zeta$ (given here in the form corrected by Högström (1988) to the use of $\kappa = 0.4$), or, in general, as

$$\phi_h(\zeta) = \text{Pr}_0 + a'_h \zeta, \qquad (B5)$$

where $\text{Pr}_0 = 0.95$ and $a_m = 7.8$. It is thus an additive formulation for the inclusion of Pr_0, which, in contrast to our formulation above, does not include the effect of Pr_0 in the stability correction term. It is obvious that after introducing $a_h\text{Pr}_0 = a'_h$ a multiplicative formulation follows, which reads $\phi_h(\zeta) = 0.95(1 + 7.8/0.95\zeta)$. Very often a'_h from (B5) is used in the framework of Eqs. (13) without a clear statement that a correction was already included.

We stress that one must clearly distinguish between the different formulations of equations concerning Pr_0. They are not interchangeable, and mixing of them can lead to erroneous results, e.g., to a dependence of ψ_h on Pr_0 in the limit $\zeta \to 0$. Recently, such pseudostability correction functions were introduced for stable conditions by Sharan et al. (2003), Sharan and Aditi (2009), and Sharan and Kumar (2010). It is in contradiction with the traditional definition [see Eq. (12)].

Finally, we note that one must also be careful with the formulation of bulk formulae for the heat flux. For example, Louis (1979) and Pithan et al. (2015) use Eq. (16) as

$$H_f = (1/\text{Pr}_0)c_p C_h |\mathbf{U}(z)|[\Theta_v(z) - \Theta_0]. \qquad (B6)$$

In this case Pr_0 would have to be skipped in Eq. (18).

APPENDIX C

Applicability of the GLGS Functions

According to Sharan and Kumar (2010) stability functions are applicable, if the inequalities (66) hold for all values of ζ in the range $0 \leq \zeta \leq \infty$. Combining Eqs. (17) with Eqs. (18), (19), and (20), the inequalities (66) can be easily reformulated in terms of stability correction functions as

$$Y_m Y'_m \geq 0, \quad Y'_m Y_h + Y_m Y'_h \geq 0, \qquad (C1)$$

where, by definition, $Y_k(\zeta) = \ln\varepsilon_k - \psi_k(\zeta) + \psi_k(\zeta/\varepsilon_k)$ with $k = [m, h]$. Equation (C1) must be valid in the range $0 \leq \zeta \leq \infty$ for all values of the given parameters ε_k. Here the prime means a partial derivative in ζ. Using the GLGS functions (34) and (35) we obtain

$$Y_m = \ln \varepsilon_m + 3 \frac{a_m}{b_m} [(1 + b_m \zeta)^{1/3} - (1 + b_m \zeta/\varepsilon_m)^{1/3}], \quad \text{(C2)}$$

$$Y_h = \ln \varepsilon_t + \mathrm{Pr}_0 \frac{a_h}{b_h} [\log(1 + b_h \zeta) - \log(1 + b_h \zeta/\varepsilon_t)], \quad \text{(C3)}$$

and

$$Y'_m = a_m [(1 + b_m \zeta)^{-2/3} - (1 + b_m \zeta/\varepsilon_m)^{-2/3}], \quad \text{(C4)}$$

$$Y'_h = \mathrm{Pr}_0 a_h [(1 + b_h \zeta)^{-1} - (1 + b_h \zeta/\varepsilon_t)^{-1}]. \quad \text{(C5)}$$

Since both $\varepsilon_m > 1$ and $\varepsilon_t > 1$ the functions Y_m and Y_h as well as Y'_m and Y'_h are always larger than 0, so that conditions (C1) are fulfilled and the transfer coefficients are decreasing functions in the whole range of $\zeta > 0$.

To summarize, we have proven that the GLGS functions are in agreement with constraint (66). Therefore, they are applicable for all values of ζ.

APPENDIX D

Sensitivity of the GLGS Functions on the Choice of Parameters

A first impression of the sensitivity of the GLGS functions on the parameters a_m, b_m, a_h, b_h, and Pr_0 can be obtained by Fig. D1 showing the ϕ_m and ϕ_h functions obtained when all parameter values are varied by ±30% relative to their optimal values given by Eq. (38). This choice of variation is in line with Webb (1970) and Högström (1996) who estimated the standard deviation for a_m and a_h as 30%. Figure D1 shows that the differences between curves for a different choice of parameters in the given limits are small compared with the scatter of the SHEBA data around the theoretical curves. This allows us some freedom for the choice of parameters.

With respect to ϕ_h a modification of Pr_0 has the largest effect. For $\zeta < 0.08$ the value of Pr_0 is by far the most important value for a good agreement with observations. As will be shown below Pr_0 affects also strongly the $\zeta(\mathrm{Ri}_b)$ relationship in this stability range. However, the first tests have been carried out without a modification of the originally chosen value $\mathrm{Pr}_0 = 0.98$.

We conclude from Fig. D1 also that the sensitivity on a_m and b_m and on a_h b_h depends on the range of considered stability. It is obvious that for $\zeta < 0.1$ the sensitivity is small compared with the sensitivity in the range $\zeta > 0.1$. Sorbjan (2017) optimized the agreement of the ϕ_m and ϕ_h functions with SHEBA data for $\zeta < 0.6$ by using $a_m = 4.7$ while G2007a proposed $a_m = 5.0$ (and $a_h = 5.0$), which formed the reason for our choice of a_m and a_h in the set of constants (38). This value is also in
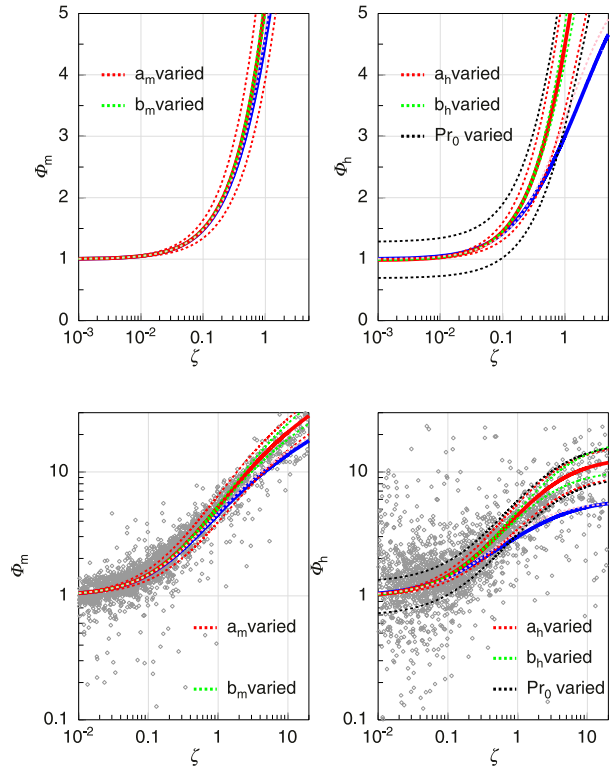

FIG. D1. Stability functions ϕ_m and ϕ_h as a function of ζ with (top) linear vertical axes and (bottom) logarithmic axes. Blue solid lines refer to the G2007a functions, while the red solid lines are the GLGS functions (32) and (33) with the optimal parameter values (38). Dashed curves represent also the GLGS functions, but with parameters a_m and a_h (red) and b_m and b_h (green) as well as P_r (black) varied by ±30% relative to their values (38). The pink dashed curves are results of the GLGS functions using the parameter values $a_m = 5.0$, $a_h = 4.3$, $b_m = 0.603$, $b_h = 0.9$, and $\mathrm{Pr}_0 = 1.0$. Individual 1-h averaged SHEBA data based on median fluxes for five levels are shown as gray symbols.

the range of the finally suggested values (a_m between 4.3 and 6.0) by Högström (1988, 1996). However, it is also obvious that especially in the near-neutral range ($\zeta < 0.02$) values of constants can vary a lot without a large effect. This motivated us to test also other values of a_m than the optimal one to obtain perhaps an improved agreement with respect to the $\zeta(\mathrm{Ri}_b)$ relation and to f_m, f_h and C_d, C_h.

Due to the above findings we tested a combination of constants assuming $a_m = 7.0$, which—as we show below—improves slightly the agreement with respect to f_m, f_h for $0.05 < \mathrm{Ri}_b < 0.2$ and for C_d and C_h in the range $0.1 < \mathrm{Ri}_b$. The value 7.0 for a_m forms an upper limit for a reasonable choice with respect to ϕ_m since a larger value would lead to larger differences (15%) to the SHEBA data especially in the near-neutral range ($\mathrm{Ri}_b < 0.05$) (not shown). For the choice $a_m = 7.0$ and $\mathrm{Pr}_0 = 0.98$ we found then the optimal set of constants
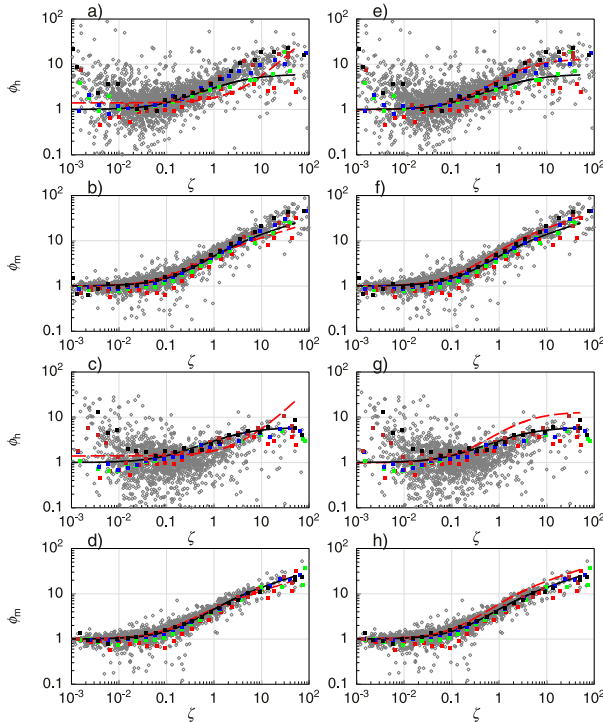
FIG. D2. As in Fig. 3, but red dashed lines represent the GLGS functions (a)–(d) using constants (D2) $a_m = 7.0$, $b_m = 1.6$, $a_h = 0.3$, $b_h = 1 \times 10^{-5}$, and $\mathrm{Pr}_0 = 1.4$ and (e)–(h) using constants (D1) $a_m = 7.0$, $b_m = 0.67$, $a_h = 5.0$, $b_h = 0.4$, and $\mathrm{Pr}_0 = 0.98$.

$$\mathrm{Pr}_0 = 0.98, \quad a_m = 7.0, \quad a_h = 5.0, \quad b_m = 0.67, \quad b_h = 0.4. \tag{D1}$$

The corresponding values of γ and ζ_a are 2.63 and 5.1. Results for ϕ_m and ϕ_h obtained with (D1) are shown in Fig. D2. The comparison with the corresponding Fig. 3 obtained with the optimal constants (38) shows only small differences. Moderate differences are visible for the $\zeta(\mathrm{Ri}_b)$ relationship (cf. Fig. 4 with Fig. D3). Namely, in the range $\mathrm{Ri}_b \approx 0.1$–0.15 the curves based on Eq. (D1) agree slightly better with the observations than the results based on (38). An improvement becomes clearer by considering the f_m and f_h functions as well as C_d and C_h, which represent the most important quantity with respect to modeling since values of transfer coefficients determine the turbulent fluxes. Figures D4 and D5 show these functions obtained with Eqs. (D1) and (38). Differences between the results occur in the range $0.01 < \mathrm{Ri}_b < 0.2$ while outside of this range there are almost no differences. For $0.01 < \mathrm{Ri}_b < 0.035$ the set of constants (D1) has slight advantages but a larger advantage for $0.035 < \mathrm{Ri}_b < 0.2$. There is especially a better agreement with the SHEBA data measured at 8.9 m height, which is closest to 10 m height, so to the level, which is mostly considered as a reference for values of transfer coefficients.
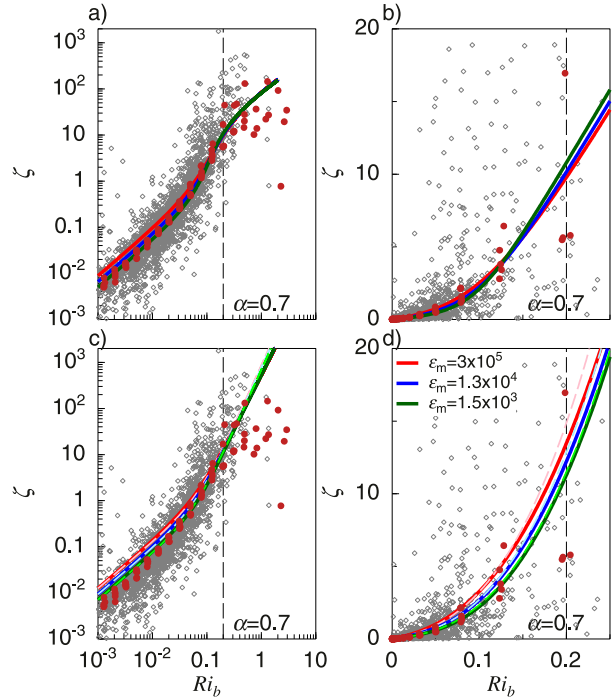

FIG. D3. As in Fig. 4, but results are based on the GLGS functions (c),(d) using constants (D1) $a_m = 7.0$, $b_m = 0.67$, $a_h = 5.0$, $b_h = 0.4$, $\mathrm{Pr}_0 = 0.98$ and (top) using constants (D2) $a_m = 7.0$, $b_m = 1.6$, $a_h = 0.3$, $b_h = 1 \times 10^{-5}$, and $\mathrm{Pr}_0 = 1.4$.

One might argue that results based on the assumption $a_m = a_h = 5.0$ could perhaps be further improved using other values for b_m and b_h than those proposed in Eq. (38). However, this leads to drawbacks as shown in Fig. D4 exemplarily for a variation of b_m.

Results are added for two further sets of parameter values. The first one is chosen as an example proving that an optimal agreement only with respect to the $\zeta(\mathrm{Ri}_b)$ relationship is not sufficient. This is interesting especially after we have shown already that vice versa an optimal fit of the ϕ functions to the corresponding SHEBA data resulted in some differences with respect to the measured and modeled transfer coefficients. An optimal agreement solely with respect to the $\zeta(\mathrm{Ri}_b)$ relationship is obtained with the parameter values

$$\mathrm{Pr}_0 = 1.4, \quad a_m = 7.0, \quad b_m = 1.6, \quad a_h = 0.3,$$
$$b_h = 1 \times 10^{-5}. \tag{D2}$$

Using these values, the $\zeta(\mathrm{Ri}_b)$ relationship is perfectly approximated in the whole range of stability (Fig. D3). However, as shown in Fig. D2 the corresponding ϕ_h functions (especially their curvature) disagree with the measurements in the range $\zeta > 1$ and this leads again to large differences to the SHEBA measurements especially for the transfer coefficients (not shown here).
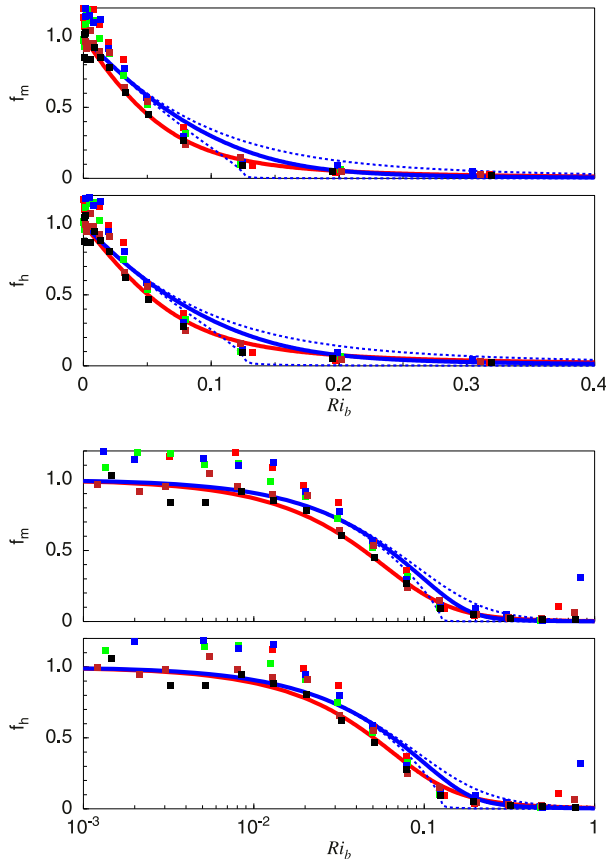
FIG. D4. Plots of f_m and f_h obtained from SHEBA (symbols with color coding as in Fig. 3) and (iterative) results based on the GLGS functions using the constants (D1) (red solid line). The blue lines represent results when $a_m = 5.0$ and $a_h = 5.0$ are prescribed and b_m and b_h are varied [blue solid line: best fit with parameters (38), upper dashed blue line: $b_m = 0.5$ and $b_h = 0.4$; lower dashed blue line: $b_m = 0.1$ and $b_h = 0.4$]. In all cases $\alpha = 0.7$.

In general, we found that the $\zeta(\mathrm{Ri}_b)$ relation in the range $\mathrm{Ri}_b < 0.05$ can be improved when Pr_0 attains values larger than 1. However, such values are not in agreement with the finding of other authors so that we do not recommend such values at the present stage of research.

There is also a set of parameter values, namely,

$$\mathrm{Pr}_0 = 1.0, \quad a_m = 5.0, \quad b_m = 0.603, \quad a_h = 4.3, \quad b_h = 0.9, \tag{D3}$$

for which the G2007a ϕ functions are ideally approximated by the GLGS functions with very small differences only (Fig. D1). Corresponding results for the $\zeta(\mathrm{Ri}_b)$ relationship and for the transfer coefficients can almost not be distinguished from those based on the original G2007a functions.

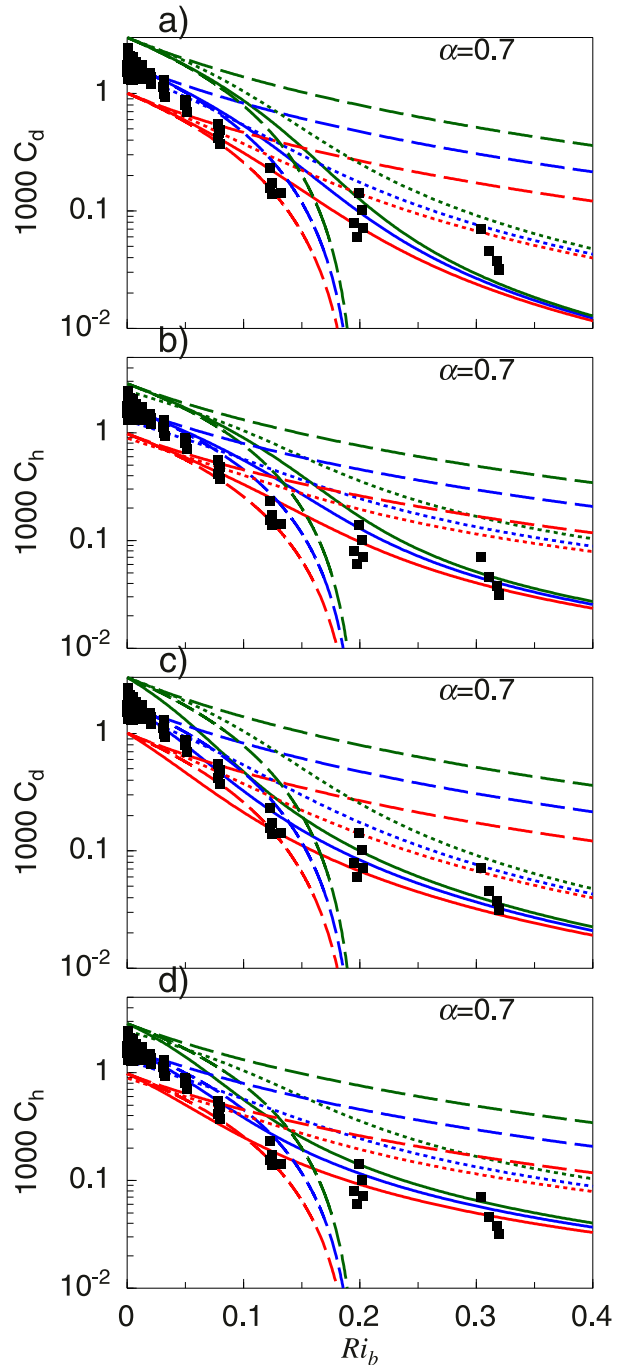FIG. D5. Transfer coefficients C_d and C_h at 10 m height as a function of Ri_b. Solid lines: based on the GLGS functions (a),(b) with the set of constants (38) ($a_m = 5.0$, $b_m = 0.3$, $a_h = 5.0$, $b_h = 0.4$, $\mathrm{Pr}_0 = 0.98$) and (c),(d) with (D1). Three lowermost dashed lines are based on the Businger–Dyer functions and three uppermost dashed lines are based on Louis (1979). Dotted lines are based on G2007a. Colors refer to different values of ε_m as in Fig. 10. Black symbols represent SHEBA measurements at different heights.

REFERENCES

Andreas, E. L., 1987: A theory for the scalar roughness and the scalar transfer coefficients over snow and sea ice. *Bound.-Layer Meteor.*, **38**, 159–184, https://doi.org/10.1007/BF00121562.

——, 2002: Parameterizing scalar transfer over snow and ice: A review. *J. Hydrometeor.*, **3**, 417–432, https://doi.org/10.1175/1525-7541(2002)003<0417:PSTOSA>2.0.CO;2.

——, C. Fairall, P. Guest, and P. O. G. Persson, 1999: An overview of the SHEBA atmospheric surface flux program. Preprints, *Fifth Conf. on Polar Meteorology and Oceanography*, Dallas, TX, Amer. Meteor. Soc., J10.1, https://ams.confex.com/ams/older/99annual/abstracts/797.htm.

——, P. O. G. Persson, A. A. Grachev, R. E. Jordan, T. W. Horst, P. S. Guest, and C. W. Fairall, 2010a: Parametrizing turbulent exchange over sea ice in winter. *J. Hydrometeor.*, **11**, 87–104, https://doi.org/10.1175/2009JHM1102.1.

——, T. W. Horst, A. A. Grachev, P. O. G. Persson, C. W. Fairall, P. S. Guest, and R. E. Jordan, 2010b: Parametrizing turbulent exchange over summer sea ice and the marginal ice zone. *Quart. J. Roy. Meteor. Soc.*, **136**, 927–943, https://doi.org/10.1002/qj.618.

Beljaars, A., and A. Holtslag, 1991: Flux parameterization over land surfaces for atmospheric models. *J. Appl. Meteor.*, **30**, 327–341, https://doi.org/10.1175/1520-0450(1991)030<0327:FPOLSF>2.0.CO;2.

Berkowicz, R., and L. P. Prahm, 1982: Evaluation of the profile method for estimation of surface fluxes of momentum and heat. *Atmos. Environ.*, **16**, 2809–2819, https://doi.org/10.1016/0004-6981(82)90032-4.

Businger, J. A., J. C. Wyngaard, Y. Izumi, and E. F. Bradley, 1971: Flux-profile relationships in the atmospheric surface layer. *J. Atmos. Sci.*, **28**, 181–189, https://doi.org/10.1175/1520-0469(1971)028<0181:FPRITA>2.0.CO;2.

Canuto, V., F. Minotti, C. Ronchi, R. Ypma, and O. Zeman, 1994: Second-order closure PBL model with new third-order moments: Comparison with LES data. *J. Atmos. Sci.*, **51**, 1605–1618, https://doi.org/10.1175/1520-0469(1994)051<1605:SOCPMW>2.0.CO;2.

Castellani, G., C. Lüpkes, S. Hendricks, and R. Gerdes, 2014: Variability of Arctic sea-ice topography and its impact on the atmospheric surface drag. *J. Geophys. Res.*, **119**, 6743–6762, https://doi.org/10.1002/2013JC009712.

Chenge, Y., and W. Brutsaert, 2005: Flux-profile relationships for wind speed and temperature in the stable atmospheric boundary layer. *Bound.-Layer Meteor.*, **114**, 519–538, https://doi.org/10.1007/s10546-004-1425-4.

Deardorff, J. W., 1968: Dependence of air-sea transfer coefficients on bulk stability. *J. Geophys. Res.*, **73**, 2549–2557, https://doi.org/10.1029/JB073i008p02549.

Delage, Y., 1997: Parameterising sub-grid scale vertical transport in atmospheric models under statically stable conditions. *Bound.-Layer Meteor.*, **82**, 23–48, https://doi.org/10.1023/A:1000132524077.

Doms, G., and Coauthors, 2011: A description of the nonhydrostatic regional COSMO model: Part II: Physical parameterization. Consortium for Small-Scale Modeling Doc., 161 pp., http://www.cosmo-model.org/content/model/documentation/core/cosmoPhysParamtr.pdf.

Dyer, A., 1974: A review of flux-profile relationships. *Bound.-Layer Meteor.*, **7**, 363–372, https://doi.org/10.1007/BF00240838.

Elvidge, A., I. Renfrew, A. Weiss, I. Brooks, T. Lachlan-Cope, and J. King, 2016: Observations of surface momentum exchange over the marginal ice zone and recommendations for its parametrisation. *Atmos. Chem. Phys.*, **16**, 1545–1563, https://doi.org/10.5194/acp-16-1545-2016.

Fairall, C., and R. Markson, 1987: Mesoscale variations in surface stress, heat fluxes, and drag coefficient in the marginal ice zone during the 1983 Marginal Ice Zone Experiment. *J. Geophys. Res.*, **92**, 6921–6932, https://doi.org/10.1029/JC092iC07p06921.

Foken, T., 2006: 50 years of the Monin–Obukhov similarity theory. *Bound.-Layer Meteor.*, **119**, 431–447, https://doi.org/10.1007/s10546-006-9048-6.

——, 2017: *Micrometeorology*. Springer, 362 pp.

Galperin, B., and S. Sukoriansky, 2010: Geophysical flows with anisotropic turbulence and dispersive waves: Flows with stable stratification. *Ocean Dyn.*, **60**, 1319–1337, https://doi.org/10.1007/s10236-010-0325-z.

Garratt, J. R., 1992: *The Atmospheric Boundary Layer*. Cambridge University Press, 316 pp.

Giorgetta, M., and Coauthors, 2012: The atmospheric general circulation model ECHAM6: Model description. Max Planck Institute Rep., 172 pp., https://www.mpimet.mpg.de/fileadmin/publikationen/Reports/WEB_BzE_135.pdf.

Grachev, A. A., E. L. Andreas, C. W. Fairall, P. S. Guest, and P. O. G. Persson, 2007a: SHEBA flux–profile relationships in the stable atmospheric boundary layer. *Bound.-Layer Meteor.*, **124**, 315–333, https://doi.org/10.1007/s10546-007-9177-6.

——, ——, ——, ——, and ——, 2007b: On the turbulent Prandtl number in the stable atmospheric boundary layer. *Bound.-Layer Meteor.*, **125**, 329–341, https://doi.org/10.1007/s10546-007-9192-7.

——, ——, ——, ——, and ——, 2008: Turbulent measurements in the stable atmospheric boundary layer during SHEBA: Ten years after. *Acta Geophys.*, **56**, 142–166, https://doi.org/10.2478/s11600-007-0048-9.

——, ——, ——, ——, and ——, 2013: The critical Richardson number and limits of applicability of local similarity theory in the stable boundary layer. *Bound.-Layer Meteor.*, **147**, 51–82, https://doi.org/10.1007/s10546-012-9771-0.

——, ——, ——, ——, and ——, 2015: Similarity theory based on the Dougherty–Ozmidov length scale. *Quart. J. Roy. Meteor. Soc.*, **141**, 1845–1856, https://doi.org/10.1002/qj.2488.

Gryanik, V. M., and C. Lüpkes, 2018: An efficient non-iterative bulk parametrization of surface fluxes for stable atmospheric conditions over polar sea-ice. *Bound.-Layer Meteor.*, **166**, 301–325, https://doi.org/10.1007/s10546-017-0302-x.

Hartmann, J., C. Kottmeier, C. Wamser, and E. Augstein, 1994: Aircraft measured atmospheric momentum, heat and radiation fluxes over Arctic sea ice. *The Polar Oceans and Their Role in Shaping the Global Environment, Meteor. Monogr.*, Vol. 85, Amer. Geophys. Union, 443–454, https://doi.org/10.1029/GM085p0443.

Högström, U., 1988: Non-dimensional wind and temperature profiles in the atmospheric surface layer: A re-evaluation. *Topics in Micrometeorology: A Festschrift for Arch Dyer*, B. B. Hicks, Eds., Springer, 55–78.

——, 1996: Review of some basic characteristics of the atmospheric surface layer. *Bound.-Layer Meteor.*, **78**, 215–246, https://doi.org/10.1007/BF00120937.

Holtslag, A., and H. De Bruin, 1988: Applied modeling of the nighttime surface energy balance over land. *J. Appl. Meteor.*, **27**, 689–704, https://doi.org/10.1175/1520-0450(1988)027<0689:AMOTNS>2.0.CO;2.

Jiménez, P. A., J. Dudhia, J. F. González-Rouco, J. Navarro, J. P. Montávez, and E. García-Bustamante, 2012: A revised scheme

for the WRF surface layer formulation. *Mon. Wea. Rev.*, **140**, 898–918, https://doi.org/10.1175/MWR-D-11-00056.1.

Jung, T., and Coauthors, 2016: Advancing polar prediction capabilities on daily to seasonal time scales. *Bull. Amer. Meteor. Soc.*, **97**, 1631–1647, https://doi.org/10.1175/BAMS-D-14-00246.1.

Launiainen, J., 1995: Derivation of the relationship between the Obukhov stability parameter and the bulk Richardson number for flux-profile studies. *Bound.-Layer Meteor.*, **76**, 165–179, https://doi.org/10.1007/BF00710895.

Li, Y., Z. Gao, D. H. Lenschow, and F. Chen, 2010: An improved approach for parameterizing surface-layer turbulent transfer coefficients in numerical models. *Bound.-Layer Meteor.*, **137**, 153–165, https://doi.org/10.1007/s10546-010-9523-y.

——, ——, D. Li, L. Wang, and H. Wang, 2014: An improved non-iterative surface layer flux scheme for atmospheric stable stratification conditions. *Geosci. Model Dev.*, **7**, 515–529, https://doi.org/10.5194/gmd-7-515-2014.

Louis, J.-F., 1979: A parametric model of vertical eddy fluxes in the atmosphere. *Bound.-Layer Meteor.*, **17**, 187–202, https://doi.org/10.1007/BF00117978.

——, M. Tiedtke, and J. Geleyn, 1981: A short history of the operational PBL-parameterization at ECMWF. *Workshop on Planetary Boundary Layer parameterization*, Reading, England, ECMWF, 59–79, https://www.ecmwf.int/node/10845.

Lüpkes, C., and V. M. Gryanik, 2015: A stability-dependent parametrization of transfer coefficients for momentum and heat over polar sea ice to be used in climate models. *J. Geophys. Res. Atmos.*, **120**, 552–581, https://doi.org/10.1002/2014JD022418.

——, ——, J. Hartmann, and E. L. Andreas, 2012: A parametrization, based on sea ice morphology, of the neutral atmospheric drag coefficients for weather prediction and climate models. *J. Geophys. Res.*, **117**, D13112, https://doi.org/10.1029/2012JD017630.

Mahrt, L., 2007: The influence of nonstationarity on the turbulent flux–gradient relationship for stable stratification. *Bound.-Layer Meteor.*, **125**, 245–264, https://doi.org/10.1007/s10546-007-9154-0.

Mauritsen, T., 2011: Advancing closures for stably stratified turbulence in global atmospheric models. *Workshop on Diurnal Cycles and the Stable Boundary Layer*, Reading, England, ECMWF, 63–74, https://www.ecmwf.int/sites/default/files/elibrary/2012/11044-advancing-closures-stably-stratified-turbulence-global-atmospheric-models.pdf.

Monin, A. S., and A. M. Obukhov, 1954: Basic laws of turbulent mixing in the atmosphere near the ground. *Tr. Geofiz. Inst., Akad. Nauk SSSR*, **24**, 163–186.

——, and A. M. Yaglom, 1971: *Statistical Fluid Mechanics*. Vols. 1 and 2. MIT Press, 874 pp.

Nieuwstadt, F. T., 1984: The turbulent structure of the stable, nocturnal boundary layer. *J. Atmos. Sci.*, **41**, 2202–2216, https://doi.org/10.1175/1520-0469(1984)041<2202:TTSOTS>2.0.CO;2.

Paulson, C. A., 1969: Comments on a paper by J. W. Deardorff, 'Dependence of air-sea transfer coefficients on bulk stability'. *J. Geophys. Res.*, **74**, 2141–2142, https://doi.org/10.1029/JB074i008p02141.

——, 1970: The mathematical representation of wind speed and temperature profiles in the unstable atmospheric surface layer. *J. Appl. Meteor.*, **9**, 857–861, https://doi.org/10.1175/1520-0450(1970)009<0857:TMROWS>2.0.CO;2.

Pithan, F., W. Angevine, and T. Mauritsen, 2015: Improving a global model from the boundary layer: Total turbulent energy and the neutral limit Prandtl number. *J. Adv. Model. Earth Syst.*, **7**, 791–805, https://doi.org/10.1002/2014MS000382.

Pleim, J. E., 2006: A simple, efficient solution of flux–profile relationships in the atmospheric surface layer. *J. Appl. Meteor. Climatol.*, **45**, 341–347, https://doi.org/10.1175/JAM2339.1.

Sandu, I., A. Beljaars, P. Bechtold, T. Mauritsen, and G. Balsamo, 2013: Why is it so difficult to represent stably stratified conditions in numerical weather prediction (NWP) models? *J. Adv. Model. Earth Syst.*, **5**, 117–133, https://doi.org/10.1002/jame.20013.

Sharan, M., and Aditi, 2009: Performance of various similarity functions for nondimensional wind and temperature profiles in the surface layer in stable conditions. *Atmos. Res.*, **94**, 246–253, https://doi.org/10.1016/j.atmosres.2009.05.014.

——, and P. Kumar, 2010: Estimation of upper bounds for the applicability of non-linear similarity functions for non-dimensional wind and temperature profiles in the surface layer in very stable conditions. *Proc. Roy. Soc.*, **467A**, 473–494, https://doi.org/10.1098/rspa.2010.0220.

——, T. V. B. P. S. Rama Krishna, and P. Aditi, 2003: Surface-layer characteristics in the stable boundary layer with strong and weak winds. *Bound.-Layer Meteor.*, **108**, 257–288, https://doi.org/10.1023/A:1024187003097.

Sidorenko, D., and Coauthors, 2015: Towards multi-resolution global climate modeling with ECHAM6-FESOM. Part I: Model formulation and mean climate. *Climate Dyn.*, **44**, 757–780, https://doi.org/10.1007/s00382-014-2290-6.

Sorbjan, Z., 1987: Comments on scaling the atmospheric boundary layer. *Bound.-Layer Meteor.*, **38**, 411–413, https://doi.org/10.1007/BF00120855.

——, 2017: Assessment of gradient-based similarity functions in the stable boundary layer derived from a large-eddy simulation. *Bound.-Layer Meteor.*, **163**, 375–392, https://doi.org/10.1007/s10546-017-0234-5.

——, and A. A. Grachev, 2010: An evaluation of the flux–gradient relationship in the stable boundary layer. *Bound.-Layer Meteor.*, **135**, 385–405, https://doi.org/10.1007/s10546-010-9482-3.

Srivastava, P., and M. Sharan, 2019: Analysis of dual nature of heat flux predicted by Monin-Obukhov similarity theory: An impact of empirical forms of stability correction functions. *J. Geophys. Res. Atmos.*, **124**, 3627–3646, https://doi.org/10.1029/2018JD029740.

——, ——, M. Kumar, and A. K. Dhuria, 2020: On stability correction functions over the Indian region under stable conditions. *Meteor. Appl.*, **27**, e1880, https://doi.org/10.1002/met.1880.

Stevens, B., and Coauthors, 2013: Atmospheric component of the MPI-M Earth system model: ECHAM6. *J. Adv. Model. Earth Syst.*, **5**, 146–172, https://doi.org/10.1002/jame.20015.

Sukoriansky, S., 2008: Implementation of the quasi-normal scale elimination (QNSE) model of stably stratified turbulence in WRF. Developmental Testbed Center Rep., 8 pp., https://dtcenter.org/sites/default/files/visitor-projects/Sukoriansky_report.pdf.

——, and B. Galperin, 2013: An analytical theory of the buoyancy–Kolmogorov subrange transition in turbulent flows with stable stratification. *Philos. Trans. Roy. Soc.*, **371A**, 20120212, https://doi.org/10.1098/rsta.2012.0212.

——, ——, and V. Perov, 2005: Application of a new spectral theory of stably stratified turbulence to the atmospheric boundary layer over sea ice. *Bound.-Layer Meteor.*, **117**, 231–257, https://doi.org/10.1007/s10546-004-6848-4.

Tastula, E.-M., B. Galperin, S. Sukoriansky, A. Luhar, and P. Anderson, 2015: The importance of surface layer parameterization in modeling of stable atmospheric boundary layers. *Atmos. Sci. Lett.*, **16**, 83–88, https://doi.org/10.1002/asl2.525.

Uttal, T., and Coauthors, 2002: Surface Heat Budget of the Arctic Ocean. *Bull. Amer. Meteor. Soc.*, **83**, 255–276, https://doi.org/10.1175/1520-0477(2002)083<0255:SHBOTA>2.3.CO;2.

van den Hurk, B. J. J. M., and A. A. M. Holtslag, 1997: On the bulk parameterization of surface fluxes for various conditions and parameter ranges. *Bound.-Layer Meteor.*, **82**, 119–134, https://doi.org/10.1023/A:1000245600901.

Vihma, T., and Coauthors, 2014: Advances in understanding and parameterization of small-scale physical processes in the marine Arctic climate system: A review. *Atmos. Chem. Phys.*, **14**, 9403–9450, https://doi.org/10.5194/acp-14-9403-2014.

Viterbo, P., A. Beljaars, J.-F. Mahfouf, and J. Teixeira, 1999: The representation of soil moisture freezing and its impact on the stable boundary layer. *Quart. J. Roy. Meteor. Soc.*, **125**, 2401–2426, https://doi.org/10.1002/qj.49712555904.

Webb, E. K., 1970: Profile relationships: The log-linear range, and extension to strong stability. *Quart. J. Roy. Meteor. Soc.*, **96**, 67–90, https://doi.org/10.1002/qj.49709640708.

Zilitinkevich, S. S., and I. N. Esau, 2007: Similarity theory and calculation of turbulent fluxes at the surface for the stably stratified atmospheric boundary layer. *Atmospheric Boundary Layers*, Springer, 37–49.

——, V. Perov, and J. King, 2002: Near-surface turbulent fluxes in stable stratification: Calculation techniques for use in general-circulation models. *Quart. J. Roy. Meteor. Soc.*, **128**, 1571–1587, https://doi.org/10.1002/qj.200212858309.

——, T. Elperin, N. Kleeorin, I. Rogachevskii, and I. Esau, 2013: A hierarchy of energy-and flux-budget (EFB) turbulence closure models for stably-stratified geophysical flows. *Bound.-Layer Meteor.*, **146**, 341–373, https://doi.org/10.1007/s10546-012-9768-8.